

# Methylation of DNA Ligase 1 by G9a/GLP Recruits UHRF1 to Replicating DNA and Regulates DNA Methylation

Laure Ferry,<sup>1,13</sup> Alexandra Fournier,<sup>1,13</sup> Takeshi Tsusaka,<sup>2,3,13</sup> Guillaume Adelmant,<sup>4</sup> Tadahiro Shimazu,<sup>2</sup> Shohei Matano,<sup>5</sup> Olivier Kirsh,<sup>1</sup> Rachel Amouroux,<sup>6,7</sup> Naoshi Dohmae,<sup>8</sup> Takehiro Suzuki,<sup>8</sup> Guillaume J. Filion,<sup>9,10</sup> Wen Deng,<sup>11</sup> Maud de Dieuleveult,<sup>1</sup> Lauriane Fritsch,<sup>1,14</sup> Srikanth Kudithipudi,<sup>12</sup> Albert Jeltsch,<sup>12</sup> Heinrich Leonhardt,<sup>11</sup> Petra Hajkova,<sup>6,7</sup> Jarrod A. Marto,<sup>4</sup> Kyohei Arita,<sup>5</sup> Yoichi Shinkai,<sup>2,\*</sup> and Pierre-Antoine Defossez<sup>1,15,\*</sup>

<sup>1</sup>Epigenetics and Cell Fate, University Paris Diderot, Sorbonne Paris Cité, UMR 7216 CNRS, 75013 Paris, France

<sup>2</sup>Cellular Memory Laboratory, RIKEN Wako, Saitama 351-0198, Japan

<sup>3</sup>Graduate School of Medicine, Diabetes, Endocrinology, and Nutrition, Kyoto University, Kyoto 606-8507, Japan

<sup>4</sup>The Blais Proteomics Center, Dana-Farber Cancer Institute, Harvard Medical School, Boston, MA 02115, USA

<sup>5</sup>Department of Medical Life Sciences, Yokohama City University, Yokohama 230-0045, Japan

<sup>6</sup>MRC Clinical Sciences Centre (CSC), Du Cane Road, London W12 0NN, UK

<sup>7</sup>Faculty of Medicine, Institute of Clinical Sciences (ICS), Imperial College London, Du Cane Road, London W12 0NN, UK

<sup>8</sup>Biomolecular Characterization Unit, Center for Sustainable Resource Science, RIKEN, Wako, Saitama 351-0198, Japan

<sup>9</sup>Centre for Genomic Regulation (CRG), The Barcelona Institute for Science and Technology, 08003 Barcelona, Spain

<sup>10</sup>Universitat Pompeu Fabra (UPF), 08002 Barcelona, Spain

<sup>11</sup>Department of Biology II and Center for Integrated Protein Science Munich (CIPSM), Ludwig-Maximilians-Universität München, 82152 Planegg-Martinsried, Germany

<sup>12</sup>Institut für Biochemie, Stuttgart University, 70569 Stuttgart, Germany

<sup>13</sup>These authors contributed equally

<sup>14</sup>Present address: CNRS UPR 1142, 34090 Montpellier, France

<sup>15</sup>Lead Contact

\*Correspondence: [yshinkai@riken.jp](mailto:yshinkai@riken.jp) (Y.S.), [pierre-antoine.defossez@univ-paris-diderot.fr](mailto:pierre-antoine.defossez@univ-paris-diderot.fr) (P.-A.D.)

<http://dx.doi.org/10.1016/j.molcel.2017.07.012>

## SUMMARY

DNA methylation is an essential epigenetic mark in mammals that has to be re-established after each round of DNA replication. The protein UHRF1 is essential for this process; it has been proposed that the protein targets newly replicated DNA by cooperatively binding hemi-methylated DNA and H3K9me2/3, but this model leaves a number of questions unanswered. Here, we present evidence for a direct recruitment of UHRF1 by the replication machinery via DNA ligase 1 (LIG1). A histone H3K9-like mimic within LIG1 is methylated by G9a and GLP and, compared with H3K9me2/3, more avidly binds UHRF1. Interaction with methylated LIG1 promotes the recruitment of UHRF1 to DNA replication sites and is required for DNA methylation maintenance. These results further elucidate the function of UHRF1, identify a non-histone target of G9a and GLP, and provide an example of a histone mimic that coordinates DNA replication and DNA methylation maintenance.

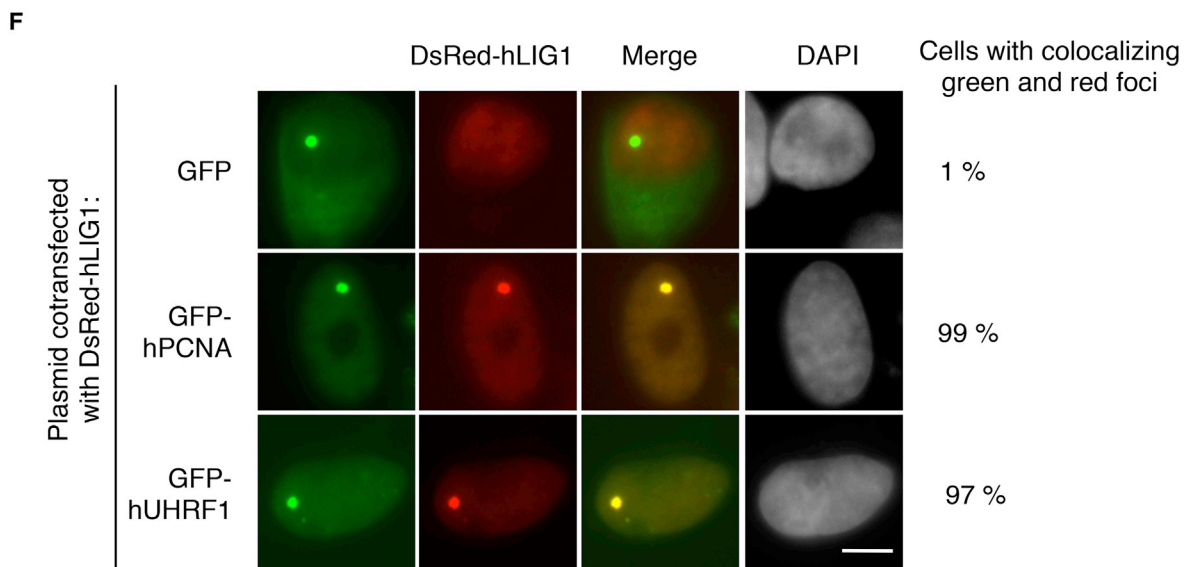
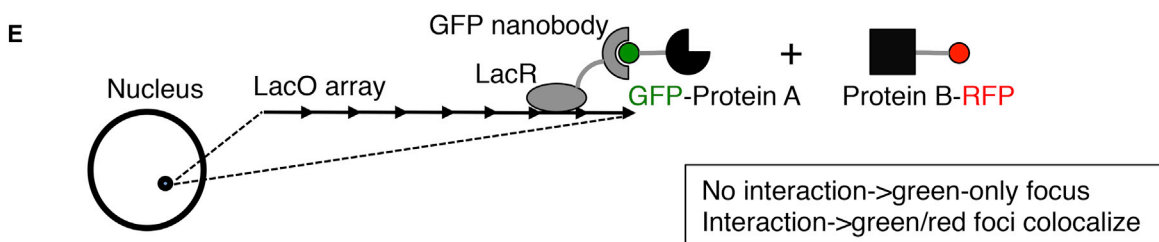
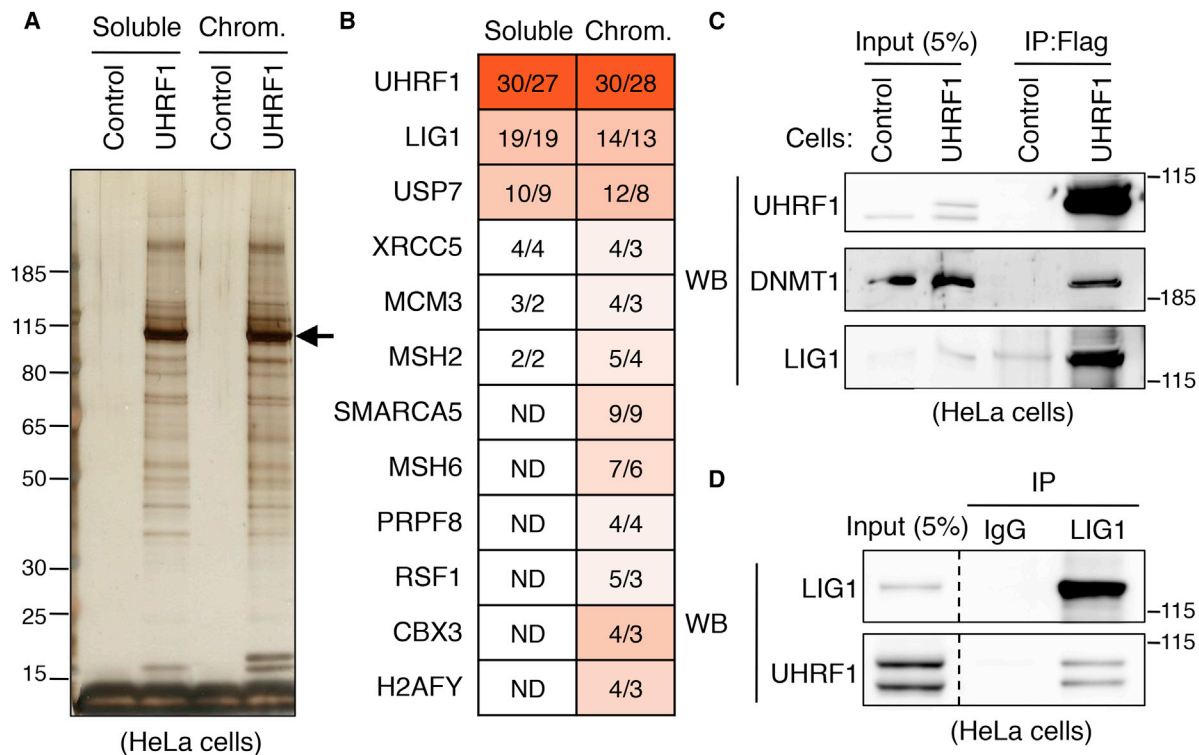
## INTRODUCTION

DNA methylation is a paradigmatic epigenetic mark with essential biological functions in mammals (Schübeler, 2015). During

DNA replication, the two symmetrically methylated strands are separated, and unmethylated DNA is synthesized, giving rise to two hemi-methylated daughter molecules. For the mark to be maintained, the hemi-methylated strands must be converted to symmetrically methylated molecules, mostly by the “maintenance” DNA methyltransferase, DNMT1 (Jeltsch and Jurkowska, 2014). This maintenance process is essential to understand, as it preserves the integrity of the epigenetic information.

The UHRF1 protein (called Np95 in mouse) binds methylated and hemi-methylated DNA via its SRA (SET-and-RING-associated) domain (Unoki et al., 2004); furthermore, in the absence of UHRF1, embryonic stem cells (ESCs) progressively lose DNA methylation (Bostick et al., 2007; Sharif et al., 2007; von Meyenn et al., 2016). Molecularly, UHRF1 interacts with DNMT1, recruits it to DNA, and stimulates its activity (Berkyurek et al., 2014; Bashtrykov et al., 2014). But how is UHRF1 itself directed to the hemi-methylated regions? A first model proposed that UHRF1 recognizes regions of recently replicated DNA simply because of its intrinsic higher affinity for hemi-methylated DNA over fully methylated DNA (Bostick et al., 2007; Sharif et al., 2007).

This model has proved valuable, but quantitative examination has suggested its potential limits. Indeed, there are roughly 25 million methyl-cytosines per genome in a differentiated human cell, the vast majority of which are in the CpG context (Lister et al., 2009). Quantitative mass spectrometry (MS) shows that there are ~30,000 molecules of UHRF1 protein per HeLa cell (Nagaraj et al., 2011). In other words, UHRF1 is largely limiting



(legend on next page)

relative to its targets, methylated and hemi-methylated CpGs. In vitro, UHRF1 binds hemi-methylated DNA ~5- to 10-fold more avidly than fully methylated CpGs (Bostick et al., 2007; Sharif et al., 2007); as the ratio of hemi-methylated to fully methylated DNA may be significantly smaller than one-tenth, especially in the early phases of DNA replication, it seems unlikely that UHRF1 can relocate to hemi-methylated CpGs just by virtue of its higher affinity for this target.

For this reason, an additional UHRF1 recruitment has been proposed to exist. In particular, another region of the protein, the tandem tudor domain (TTD), was found to be necessary for DNA methylation maintenance (Rothbart et al., 2013; Liu et al., 2013b). As the TTD binds H3K9me2/3 (Rottach et al., 2010; Nady et al., 2011), it was hypothesized that joint recognition of hemi-methylated DNA by the SRA domain, and of H3K9me2/3 by the TTD, allows efficient targeting of UHRF1 to its sites. In agreement with this, the enzymes G9a and GLP (also known as Ehmt2 and Ehmt1, respectively), which are required for H3K9 methylation, are also required for DNA methylation at some loci (Tachibana et al., 2008; Dong et al., 2008).

This new model also has limitations. First, there are ~30 million nucleosomes in a human nucleus (Nagaraj et al., 2011), of which ~50% bear H3K9me2/3, therefore potentially saturating UHRF1 binding (Cuomo et al., 2011). In this situation, how can UHRF1 be directed specifically to the nucleosomes of newly replicated chromatin? In addition, the model does not explain how UHRF1 promotes remethylation in regions that have low levels of H3K9me2/3 altogether, and which constitute ~50% of the non-repeated genome in mouse ESCs (mESCs) (von Meyenn et al., 2016).

With this in mind, we have sought to better understand UHRF1 in DNA methylation maintenance. We find that a replication protein, DNA ligase 1 (LIG1), is a prevalent and direct interactor of UHRF1. The interaction is mediated by a histone mimic within LIG1, methylated by G9a and GLP, which binds the TTD of UHRF1 in a methylation-dependent manner, and we show that this mechanism plays a direct role in the recruitment of UHRF1 to replication foci and in DNA methylation maintenance. Our results prompt a re-evaluation of the proposed mechanism of action for UHRF1, and especially the function of its TTD. They also bring to light a new non-histone target of G9a and GLP that may be involved in their role in DNA methylation regulation. Finally, they establish the first example of a histone mimic coordinating DNA replication and DNA methylation maintenance.

## RESULTS

### The UHRF1 Complex Contains DNA Ligase 1

To isolate the UHRF1 complex, we developed a HeLa cell line stably expressing HA-FLAG-UHRF1; the exogenous protein is nuclear (Figures S1A and S1B) and expressed at a level lower than the endogenous UHRF1 protein (Figure S1C). The “soluble nuclear” and “chromatin” fractions prepared from these cells were submitted to tandem immunoprecipitation (Figure 1A), followed by MS (Figures 1B and S1D). As expected, we recovered several known interactors of UHRF1, such as USP7 (Felle et al., 2011) (Figure 1B), DNMT1, and HDAC1 (Du et al., 2010) (Figure S1D). We focused our attention for further studies on DNA ligase1 (LIG1).

### UHRF1 Interacts with DNA Ligase 1

Next, we verified that LIG1 co-immunoprecipitated with HA-FLAG-tagged UHRF1 in our stable cell line (Figure 1C). Interaction occurred even in the presence of ethidium bromide (EtBr); thus, it is not mediated by DNA. In the reciprocal experiment, UHRF1 also co-immunoprecipitated with endogenous LIG1 (Figure 1D).

We also assessed the interaction by an independent approach, the fluorescent three-hybrid assay (F3H) (Figure 1E) (Herce et al., 2013). The negative control, GFP, was efficiently recruited to the LacOp array, but failed to attract DsRed-hLIG1 (Figure 1F). The positive control GFP-PCNA, a known interactor of LIG1 (Levin et al., 1997), recruited DsRed-hLIG1 in 99% of cells. When GFP-UHRF1 was co-transfected with DsRed-hLIG1, 97% of the transfected cells showed a red focus co-localizing with the GFP-UHRF1 focus. In this experiment, we can distinguish cells in S phase (they have LIG1 foci) from cells outside of S phase. The interaction between UHRF1 and LIG1 was seen in all cells examined, showing that it is not limited to S phase.

These data show that UHRF1 and LIG1 are present in a complex that does not require DNA.

### The Tandem Tudor Domain of UHRF1 Mediates the Interaction with LIG1

UHRF1 has five known protein domains: the ubiquitin-like (Ubl), plant homeo domain (PHD), tandem tudor domain (TTD), SET-and-RING associated (SRA), and really interesting new gene (RING) domains (Figure 2A). We cloned each as a GFP fusion and tested their interaction with LIG1.

#### Figure 1. UHRF1 and LIG1 Interact

(A) The proteins associated with UHRF1 were purified by tandem immunoprecipitation, separated by SDS-PAGE, and revealed by silver staining. HA-FLAG-UHRF1 is indicated by an arrowhead.

(B) LIG1 is a major component of the UHRF1 complex. Protein partners of UHRF1 in the soluble nuclear and chromatin extracts were identified by LC-MS/MS. Their abundance relative to UHRF1 was quantified by a label-free approach and color-coded from red to white. The number of peptides detected in each of the two technical replicates is also indicated. ND, no data.

(C) LIG1 co-immunoprecipitates with HA-FLAG-UHRF1. DNMT1 is used as a positive control.

(D) Endogenous LIG1 immunoprecipitates both endogenous and HA-FLAG-UHRF1.

(E) Principle of the fluorescent-3-hybrid (F3H) assay.

(F) The F3H assay confirms the interaction between UHRF1 and LIG1. PCNA is used as a positive control for LIG1 binding. n = 100 cells scored in at least two independent experiments in this and all subsequent F3H data. Scale bar, 5  $\mu$ m. Human proteins are denoted with an h (e.g., hLIG1) and mouse proteins with an m (e.g., mLIG1).

See also Figure S1.

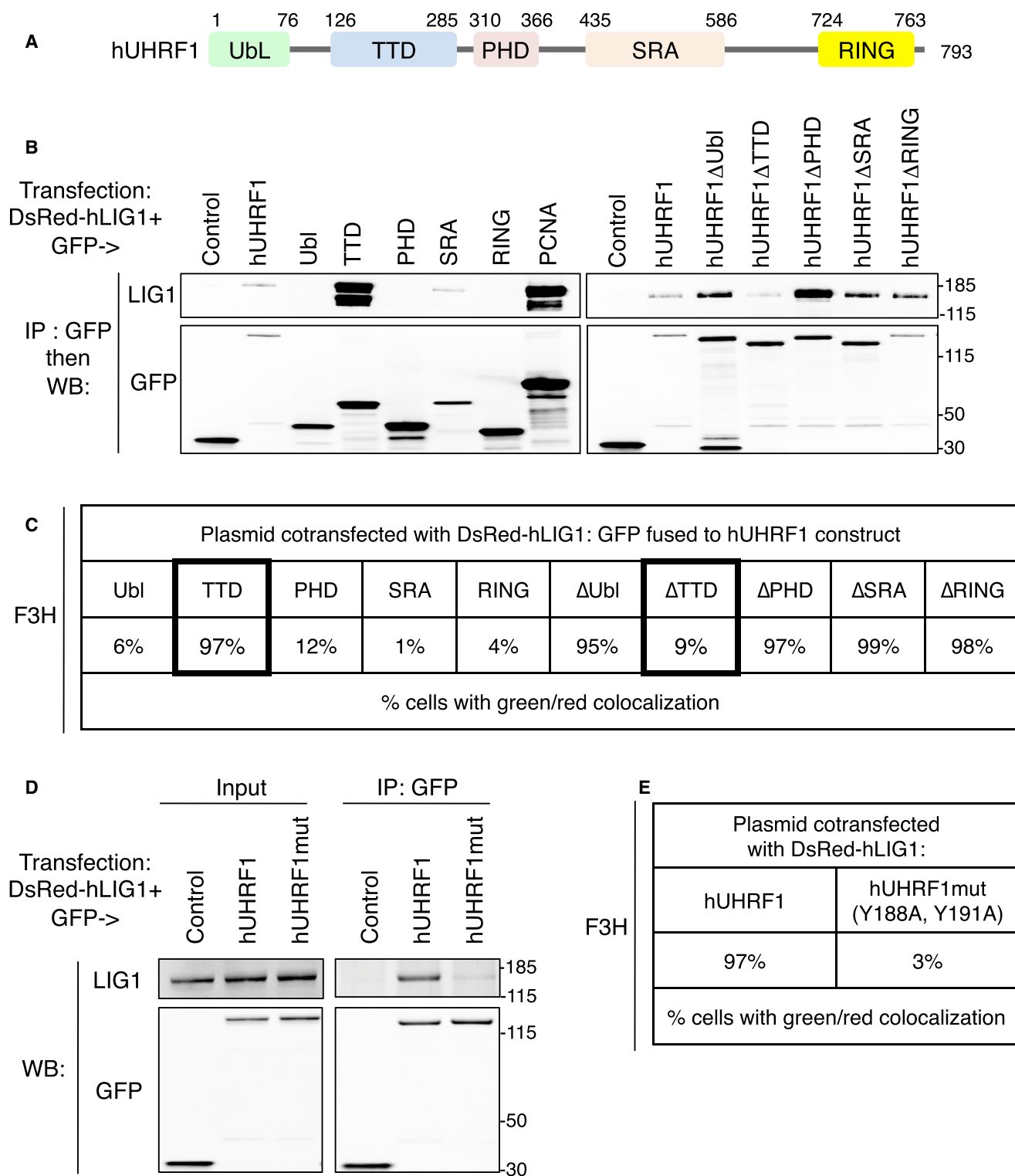


**Figure 2. The Histone-Binding Interface of the Tandem Tudor Domain Mediates the Interaction of UHRF1 with LIG1**

(A) The human UHRF1 protein.

(B) The TTD of UHRF1 is sufficient and necessary for co-immunoprecipitation with LIG1.

(legend continued on next page)

We found in co-immunoprecipitation (with EtBr) that the TTD interacted robustly with DsRed-hLIG1 (Figures 2B and S2A). We also found that only the deletion of the TTD significantly reduced the UHRF1/LIG1 interaction: the  $\Delta$ Ubl,  $\Delta$ PHD,  $\Delta$ SRA, and  $\Delta$ RING derivatives of UHRF1 could all efficiently precipitate DsRed-hLIG1, in contrast with the  $\Delta$ TTD protein (Figures 2B and S2A). F3H yielded highly similar results (Figures 2C, S2B, and S2C). Therefore, the TTD of UHRF1 is necessary and sufficient to mediate the co-immunoprecipitation with LIG1.

The TTD has a tightly packed pair of tudor domains, each with a five-stranded beta-barrel fold (Arita et al., 2012). The N-terminal tudor domain accommodates the methylated lysine of H3K9me2/3 in a hydrophobic pocket formed by Y188 and Y191 (Rottach et al., 2010; Nady et al., 2011; Rothbart et al., 2012, 2013). To test whether this pocket is also important for LIG1 binding, we generated a GFP-UHRF1mut construct harboring the Y188A/Y191A double mutation; this mutant was strongly affected for LIG1 interaction in co-immunoprecipitation (Figure 2D) and F3H (Figure 2E).

Altogether these results establish that the TTD of UHRF1 is necessary and sufficient for interaction with LIG1. Point mutations that abolish the binding of UHRF1 to methylated H3K9 also abolish the binding of UHRF1 to LIG1, suggesting that the binding interface is similar in the two cases.

### A Histone H3 Mimic within LIG1 Mediates Its Interaction with UHRF1

LIG1 has four identifiable domains: an N-terminal PCNA-binding domain (PBD) and a C-terminal catalytic region made of a DNA-binding domain, an adenylation domain, and an OB fold (Figure 3A). F3H showed that the non-catalytic part of LIG1 (amino acids [aa] 1–260) was both necessary and sufficient for the recruitment to UHRF1 foci (Figure 3B). Deletions showed that the region 112–178 was both necessary and sufficient for LIG1 to interact with UHRF1 (Figure 3B).

Visual inspection of this sequence revealed the presence of a histone-like motif similar to the N terminus of histone H3 (Figure 3C). This motif, containing the sequence “TARK,” is highly conserved throughout evolution, and was found in all vertebrates examined, as well as some invertebrates, such as *Ciona intestinalis* (Figure 3C). Methylated H3K9 is a known ligand of UHRF1’s TTD, so we tested whether an equivalent residue in LIG1, K126, was required for binding to UHRF1. K126A and K126R mutations drastically reduced the ability of LIG1 to co-localize with UHRF1 in F3H (Figure 3D and S3A), suggesting that LIG1K126 is indeed critical for the interaction. In contrast, mutation of LIG1K795, a residue that is methylated (Moore et al., 2013), had no effect on the interaction of LIG1 with UHRF1 (Figure 3D and S3A). Co-immunoprecipitation further supported the importance of LIG1K126 for UHRF1, but not PCNA, interaction (Figures 3E and S3B–S3D).

We also verified our findings on endogenous proteins in mESCs. Using CRISPR, we generated two independent lines

with mutations in *Lig1* (Figure 3F). In cells *Lig1* $\Delta$ 32, one allele is inactivated and the cDNAs made by the other allele skip one coding exon containing 96 base pairs. As a consequence, the *Lig1* $\Delta$ 32 line expresses a shorter version of LIG1 missing the 32 amino acids immediately following the T in the TARK motif. cDNAs produced in line *Lig1* $\delta$ 66 skip the same exon as well as the following exon (containing 102 base pairs), resulting in the production of a shorter LIG1 protein lacking 66 amino acids, and that is also devoid of the TARK motif. All cell lines have comparable growth characteristics, cell-cycle distribution, and gamma-H2AX content, indicative of functional replication machinery (see Figure S8 for full clone characterization). We found that wild-type (WT) mLIG1 efficiently co-immunoprecipitated UHRF1 in ESCs, whereas the two mutant forms mLIG1 $\Delta$ 32 and mLIG1 $\Delta$ 66 did so very poorly, yet interacted normally with PCNA (Figure 3G). Altogether, these results show that the histone mimic within LIG1 is necessary for interaction with UHRF1.

### The Interaction between the UHRF1 TTD and the LIG1 Histone Mimic Is Direct and Increased by Lysine Methylation

We then asked whether endogenous LIG1K126 was methylated in cells using immunoprecipitation and MS (Figure 4A). LIG1K126 was indeed methylated in human HEK293T cells: only ~25% of K126 was unmethylated, and K126me2 was the most abundant methylated form (>50% of the total), followed by K126me1 (20.1%) and K126me3 (<5%). In mESCs, methylation of the homologous residue (K142) was also prevalent, with <5% unmethylated form, and a majority of di-methylated molecules (70.6%) (Figure 4A).

Next, we asked whether a peptide with the LIG1 histone mimic would interact directly with recombinant TTD, and whether this would be modified by lysine methylation. For this, we first used native electrophoretic mobility shift assay (EMSA) (Figure 4B). The binding of methylated hLIG1 peptides was indeed considerably enhanced over unmethylated peptides.

Next, we quantified this interaction. In fluorescence polarization experiments, LIG1K126 methylation increased its binding to the UHRF1 TTD: after methylation, the Kd decreased from 900 to 40–80 nM (Figure 4C). Isothermal titration calorimetry gave similar results (Figure S4A). We also assayed the full-length UHRF1 molecule; it bound hLIG1K126me1 and hLIG1K126me3 peptides with an affinity similar to H3K9me3 peptides, and it bound hLIG1K126me2 peptides 4-fold more avidly than H3K9me3 peptides. The binding to hLIG1 was not enhanced by the presence of hemi-methylated DNA (Figure S4B).

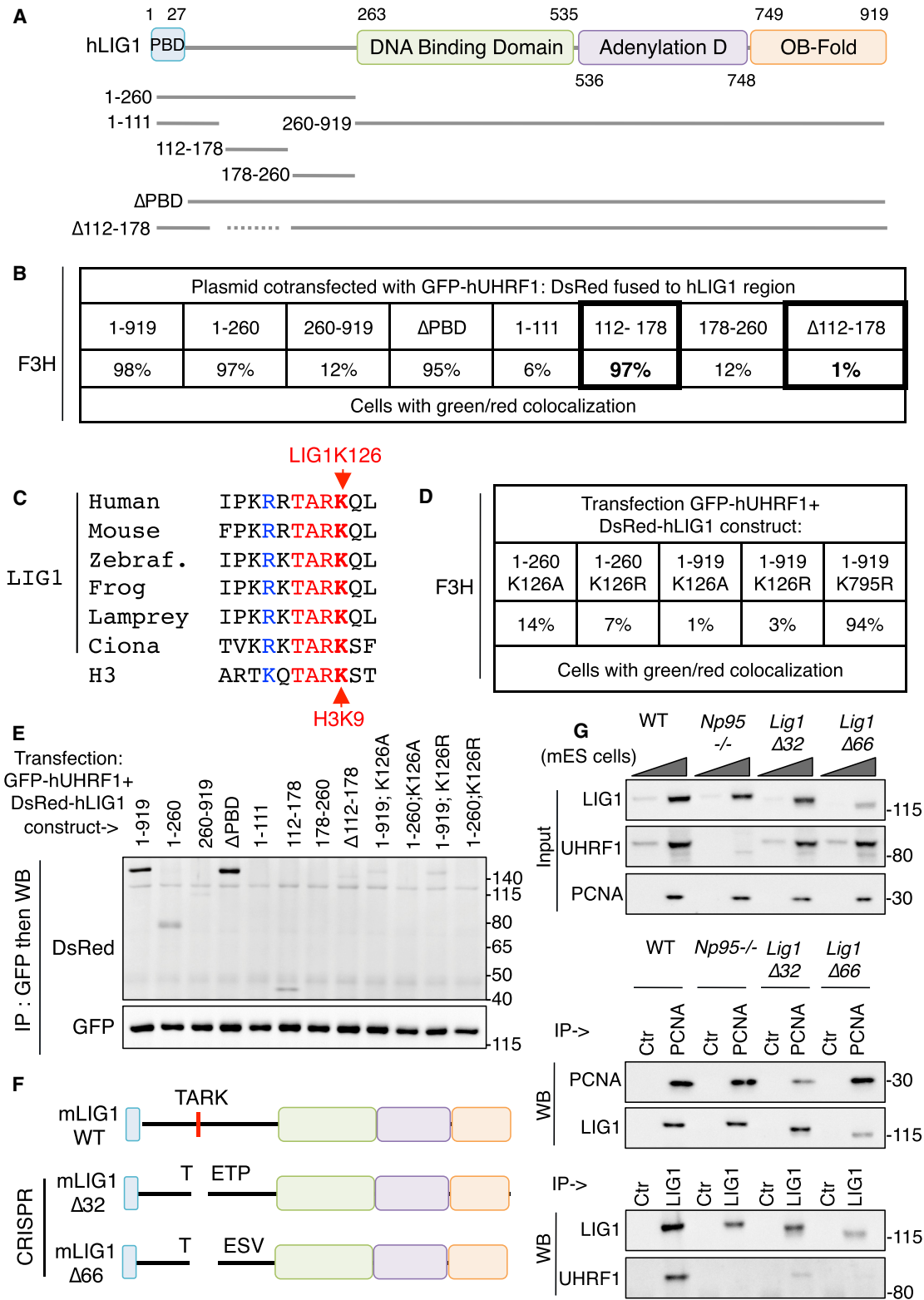
We performed homology modeling using the published TTD/H3K9me3 crystal structure (Nady et al., 2011). It suggested that the LIG1 peptide could bind UHRF1 similarly to H3, with methylated LIG1K126 interacting with the hydrophobic pocket formed by UHRF1F152, Y188, and Y191 (Figures 4D and 4E). Consistently, a Y188A/Y191A mutant TTD failed to interact with LIG1 (Figure S4C). The modeling also suggested an

(C) F3H confirms that the TTD of UHRF1 mediates the interaction with LIG1.

(D) Mutating the methyl-lysine-binding pocket of the TTD prevents interaction of UHRF1 with LIG1. UHRF1mut has the two mutations Y188A/Y191A.

(E) F3H confirms that the methyl-lysine-binding pocket is necessary for interaction with LIG1.

See also Figure S2.



(legend on next page)

important role of UHRF1D142 in the interaction with LIG1, which was confirmed experimentally (Figure S4C).

Together, these data show that LIG1 interacts with UHRF1 in a methylation-dependent manner, with an affinity equal to or greater than that of methylated H3K9.

### G9a and GLP Methylate the LIG1 Histone Mimic In Vitro and in Cells

G9a and GLP are two related lysine methyltransferases that promote the mono-, di-, and tri-methylation of H3K9 in vitro (Shinkai and Tachibana, 2011). As they can also target some non-histone proteins (e.g., Sampath et al., 2007; Rathert et al., 2008), we asked whether the enzymes might act on LIG1. Both enzymes efficiently methylated a recombinant N-terminal fragment of human LIG1 (aa 1–230), but not when the recombinant protein contained a K126A or K126R substitution (Figure 5A). G9a and GLP also methylated the full-length recombinant human LIG1 (Figure S5A), as well as mouse LIG1 on the homologous residue, K142 (data not shown).

Liquid chromatography-tandem mass spectrometry (LC-MS/MS) and MS/MS established that K126 is the residue modified by G9a and GLP, and that it is di- and tri-methylated in vitro (Figures S5B and S5C). We also raised monoclonal antibodies against LIG1K126me2 and LIG1K126me3. They did not recognize H3K9 or H3K27 methylation in ELISA and western blotting (see Figure S9 for full antibody characterization); an in vitro time course methylation assay further supported their specificity (Figure S5D).

We then used these antibodies for western blotting on mESCs mutant for *G9a*, *Glp*, or both (Figure 5B). A pan-LIG1 antibody showed that all lines expressed similar amounts of LIG1. The anti-LIG1K126me2 antibody gave high signal in the WT cells, reduced signal in either *G9a*<sup>-/-</sup> or *Glp*<sup>-/-</sup> mutant cells, and undetectable signal in the *G9a/Glp* double-knockout (DKO) cells (Figure 5B). The anti-LIG1K126me3 antibody gave weak signal in the WT cells, higher signal in the *G9a*<sup>-/-</sup> cells, and no signal in the *Glp*<sup>-/-</sup> or *G9a/Glp* DKO cells. MS was concordant, with an increase of LIG1K126me3 in the *G9a*<sup>-/-</sup> cells, and a disappearance of LIG1K126me3 in the *Glp*<sup>-/-</sup> or *G9a/Glp* DKO cells (Figure S5E). Therefore, the activity of either G9a or GLP is necessary for LIG1 methylation in mESCs. In contrast, LIG1 methylation was not affected by the absence of the methyltransferases SETDB1, or SUV39H1 and SUV39H2 (Figure S5F).

Consistent with our previous data, we found decreased UHRF1/LIG1 co-immunoprecipitation in mutant cells, especially those lacking *Glp* or both *G9a* and *Glp* (Figure 5C), which have the least LIG1K126 methylation (Figure S5E).

Another prediction was that treating cells with a G9a/GLP inhibitor should inhibit the LIG1/UHRF1 interaction; we therefore

treated human HeLa cells with UNC0642 (Liu et al., 2013a). As expected, the treatment reduced both di- and tri-methylation of LIG1K126 (Figure 5D); it also decreased the LIG1/UHRF1 interaction both in co-immunoprecipitation (Figure 5E) and F3H (Figure 5F).

Together, these results show that G9a and GLP methylate LIG1K126 in vitro and are necessary for the methylation to occur in cells. Furthermore, inhibiting this methylation by a chemical inhibitor or genetic means decreases the interaction between LIG1 and UHRF1.

### The Interaction with LIG1 Promotes UHRF1 Recruitment to Replication Foci

Next, we asked whether LIG1 can influence UHRF1 localization in cells. For this, we cotransfected the proteins tagged with fluorescent moieties in human cells. UHRF1 and LIG1 co-localized at replication foci (marked by EdU incorporation) in untreated cells (Figure 6A). In contrast, in cells treated with the G9a/GLP inhibitor UNC0642, LIG1 still co-localized with replication foci, but UHRF1 failed to be recruited to these foci (Figure 6A).

In this same assay, the TTD of UHRF1, expressed on its own, co-localized with LIG1 at foci (Figure 6B); no other UHRF1 domain did (data not shown). Mutating the hydrophobic cage of the TTD prevented recruitment to replication foci (Figure 6B). Finally, deleting the TTD from UHRF1 prevented its recruitment to LIG1 foci, whereas all other domains were dispensable (data not shown). These data could be explained by the TTD being recruited at replication foci by methylated H3K9, or methylated LIG1K126, or both. To discriminate, we used a K126R hLIG1 mutant (Figure 6C): this protein correctly localized at replication foci, but did not promote UHRF1 recruitment, arguing that the TTD is indeed recruited to the replication foci by LIG1.

We next assessed the distribution pattern of endogenous UHRF1 and LIG1 in ESCs. First, using the antibody described above, we found that LIG1K126me2 was concentrated at EdU foci, whereas the same antibody used in *G9a/Glp* DKO gave no detectable staining (Figure 6D), consistent with our previous MS and western blotting data. These data show that K126-dimethylated LIG1 molecules are present at replicating regions.

We then examined UHRF1 distribution: the protein formed nuclear foci in some cells, which systematically co-localized with the DAPI-dense chromocenters. In particular, replicating chromocenters (marked by EdU) showed bright UHRF1 foci in approximately two-thirds of WT cells. In contrast, in cells with the *Lig1Δ32*, the *Lig1Δ66* mutation, or a complete *Lig1* KO, significantly fewer replicating chromocenters were UHRF1 positive (representative images in Figure S6A; quantitation in Figures 6E and S6B). Importantly, the mLIG1Δ32 and mLIG1Δ66

### Figure 3. An H3-like Histone Mimic within LIG1 Mediates Interaction with UHRF1

- (A) The human LIG1 protein.  
 (B) F3H shows that the region 112–178 of hLIG1 is sufficient and necessary for binding to UHRF1.  
 (C) The region 112–178 of hLIG1 contains a conserved H3-like histone mimic, where LIG1K126 is analogous to H3K9.  
 (D) F3H shows that LIG1K126 is necessary for interaction with UHRF1.  
 (E) Co-immunoprecipitation confirms the importance of LIG1K126 for interaction with UHRF1.  
 (F) The LIG1 mutant forms expressed by ESC CRISPR clones mLIG1Δ32 (lacking aa 127–158) and mLIG1Δ66 (lacking aa 127–192).  
 (G) Mutant LIG1 protein lacking the TARK motif inefficiently interacts with UHRF1. Endogenous co-immunoprecipitation using the cells depicted in (F).  
 See also Figures S3 and S8.

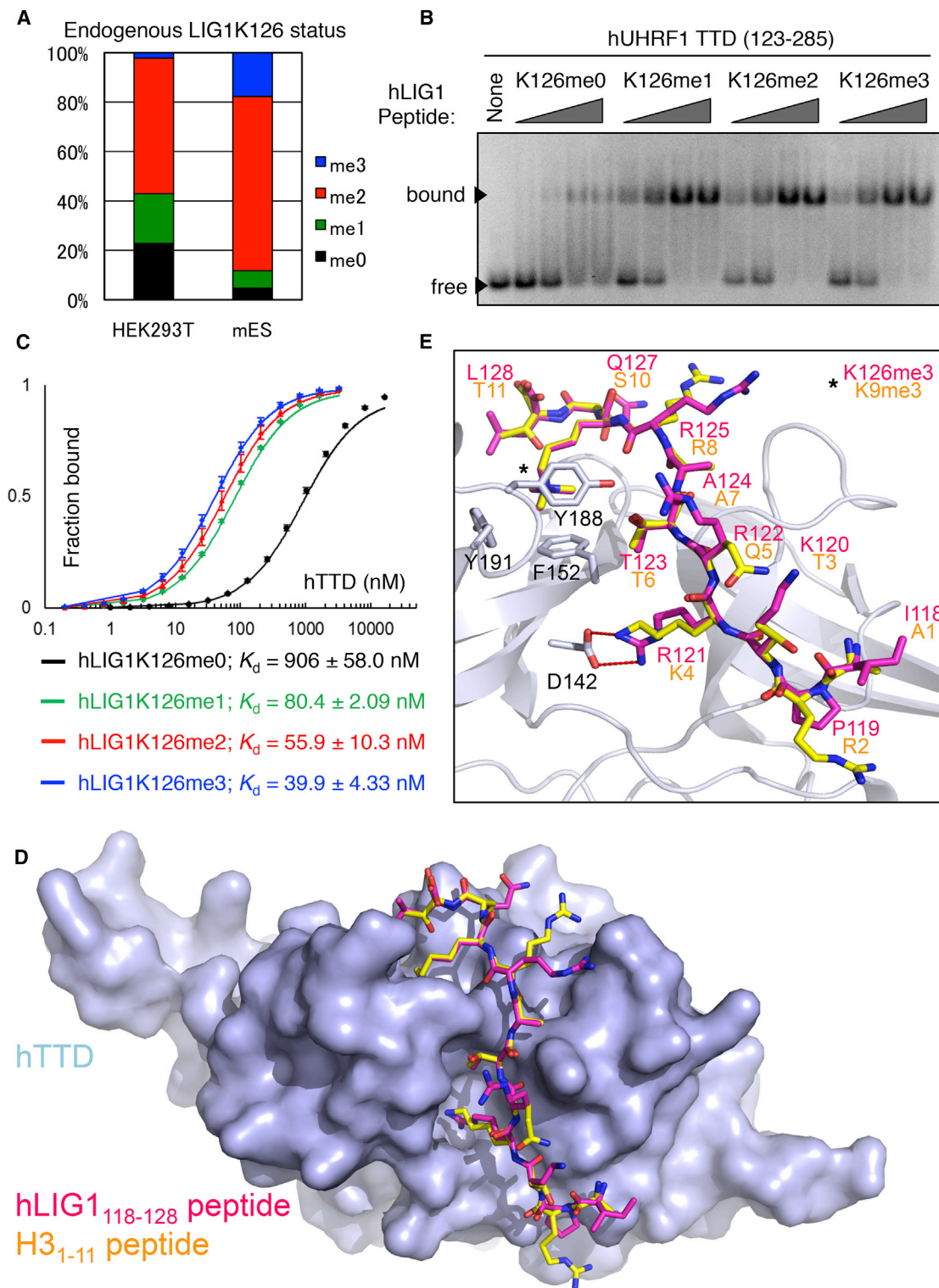


**Figure 4. LIG1K126 Is Methylated in Cells; the Interaction between the LIG1 Histone Mimic and UHRF1 Is Direct and Stimulated by Lysine Methylation**

(A) Percentage of unmethylated and methylated forms of LIG1K126 in human HEK293T and mESCs, as estimated by LIG1 immunoprecipitation and MS.

(B) Native EMSA shows an interaction between the UHRF1 TTD and K126-methylated LIG1 peptides.

(C) Fluorescence polarization experiments. Vertical axis, level of binding (fraction bound); horizontal axis, protein concentration (nM).

(legend continued on next page)

proteins still co-localized with EdU at chromocenters in most cells (Figures S6C and S10A). Also, the LIG1K126me2 form is detected at replication foci of WT cells, but not in *Lig1Δ32* or *Lig1Δ66* cells (Figure S6D).

Re-expressing WT mLIG1 in *Lig1Δ32* cells led to increased UHRF1 recruitment at replicating chromocenters, whereas expressing an mLIG1K142R mutant did not (Figure 6E). We also examined DNMT1 distribution in cells with mutated LIG1 and observed highly concordant effects (Figures 6E and S6B). Of note, the protein expression levels of UHRF1 and DNMT1, and the H3K9 methylation status, were not altered in the *Lig1* mutant cell lines (Figure S6F). These data demonstrate that LIG1 containing the H3-like motif promotes UHRF1 and DNMT1 recruitment to replicating heterochromatin in ESCs.

Next, we tested the role of G9a and GLP by assessing endogenous UHRF1 co-localization with EdU foci: we found that it was affected after the deletion of *G9a*, *Glp*, or both (Figure 6F; representative images in Figure S6E). The effect of *G9a* deletion was relatively mild, whereas the effect of deleting *Glp* or both *G9a* and *Glp* was much stronger; importantly, this correlated with the degree of LIG1K126, but not H3K9 methylation in these cells (Figure 5B), arguing that the decreased recruitment is indeed due to LIG1K126 methylation. In *G9a/Glp* DKO cells, which lack both H3K9me2 and LIG1K126 methylation, the distribution of UHRF1 was particularly diffuse, without any apparent recruitment to chromocenters. Again, the distribution of DNMT1 resembled that of UHRF1 in the cells lacking *G9a*, *Glp*, or both (Figure 6F, lower panel). In contrast, endogenous LIG1 recruitment to replication foci was not altered by the absence of *G9a* and/or *GLP* (Figures S6G and S10B). The protein expression levels of UHRF1 and DNMT1 were slightly decreased in the absence of *G9a* and/or *GLP*, but were comparable between the three mutant lines (Figure S6H).

These data show that methylated LIG1 promotes UHRF1 recruitment to replicating regions. This recruitment fails to occur in the absence of *G9a* and *GLP* activity, with a particular dependence on *GLP*.

### Disturbing the LIG1/UHRF1 Interaction Causes a Loss of DNA Methylation in ESCs

Last, we sought to investigate the relevance of the UHRF1/LIG1 interaction for DNA methylation. For this, we used independent methods to examine DNA methylation in the ESC CRISPR clones described earlier. We first used a global approach that precisely quantifies 5-methylcytosine (5mC) abundance in DNA: LC-MS/MS (Amouroux et al., 2016). We used as a control E14 *Np95*<sup>-/-</sup> mESCs (Sharif et al., 2007); as expected, they had a decreased 5mC amount (50% less; Figure 7A). The mutant cells expressing LIG1 protein that cannot interact with UHRF1 also had a significant decrease of 5mC (~30% less in clone *Lig1Δ32* and ~25% less in *Lig1Δ66*; Figure 7A). Surprisingly, the cells completely lacking LIG1 (*Lig1*<sup>-/-</sup>) had no detectable loss of DNA methylation (Figure 7A),

suggesting that a backup methylation mechanism may operate when LIG1 is missing (see the Discussion).

We then performed a luminometric methylation assay (LUMA), which uses pyrosequencing to determine the average methylation level at CCGG sites in the genome. With this approach, we again saw a significant decrease of DNA methylation in *Lig1Δ32* and *Lig1Δ66* mutant cells (Figure 7B). IAP repeats are heavily methylated in a UHRF1-dependent manner (Sharif et al., 2007). We therefore tested whether their methylation was affected by LIG1 mutation using methylation-sensitive restriction enzymes and southern blotting. Again, we saw decreased methylation in the *Lig1Δ32* and *Lig1Δ66* mutant cells (Figure S7A).

Next, we used reduced representation bisulfite sequencing (RRBS) (Gu et al., 2011). At least 30 million sequences were obtained for each line: the mapping efficiency was ~68%, the conversion efficiency was greater than 99.5%, and the number of CpGs analyzed for each line was ~100 million (see Figure S7B); of those, ~1.5 million CpGs were covered at least 10 times in every sample with a Phred quality score >20 (“high-quality CpGs” in Figure 7C) and were used for further comparative analysis. As expected, we observed significant methylation changes in the *Np95*<sup>-/-</sup> mutant cells compared to WT, with  $2.7 \times 10^5$  sites differentially methylated relative to WT with a q value of 5% or less, of which ~99% experienced demethylation (Figures 7C and 7D). Intergenic regions and introns were over-represented in the demethylated regions (Figure 7E). The mutants *Lig1Δ32* and *Lig1Δ66* also showed demethylation, affecting the same type of regions (Figures 7D and 7E). In addition, the sites demethylated in *Lig1Δ32* and *Lig1Δ66* were also demethylated in *Np95*<sup>-/-</sup> cells (Figure 7F). These data were validated by pyrosequencing (Figure S7C).

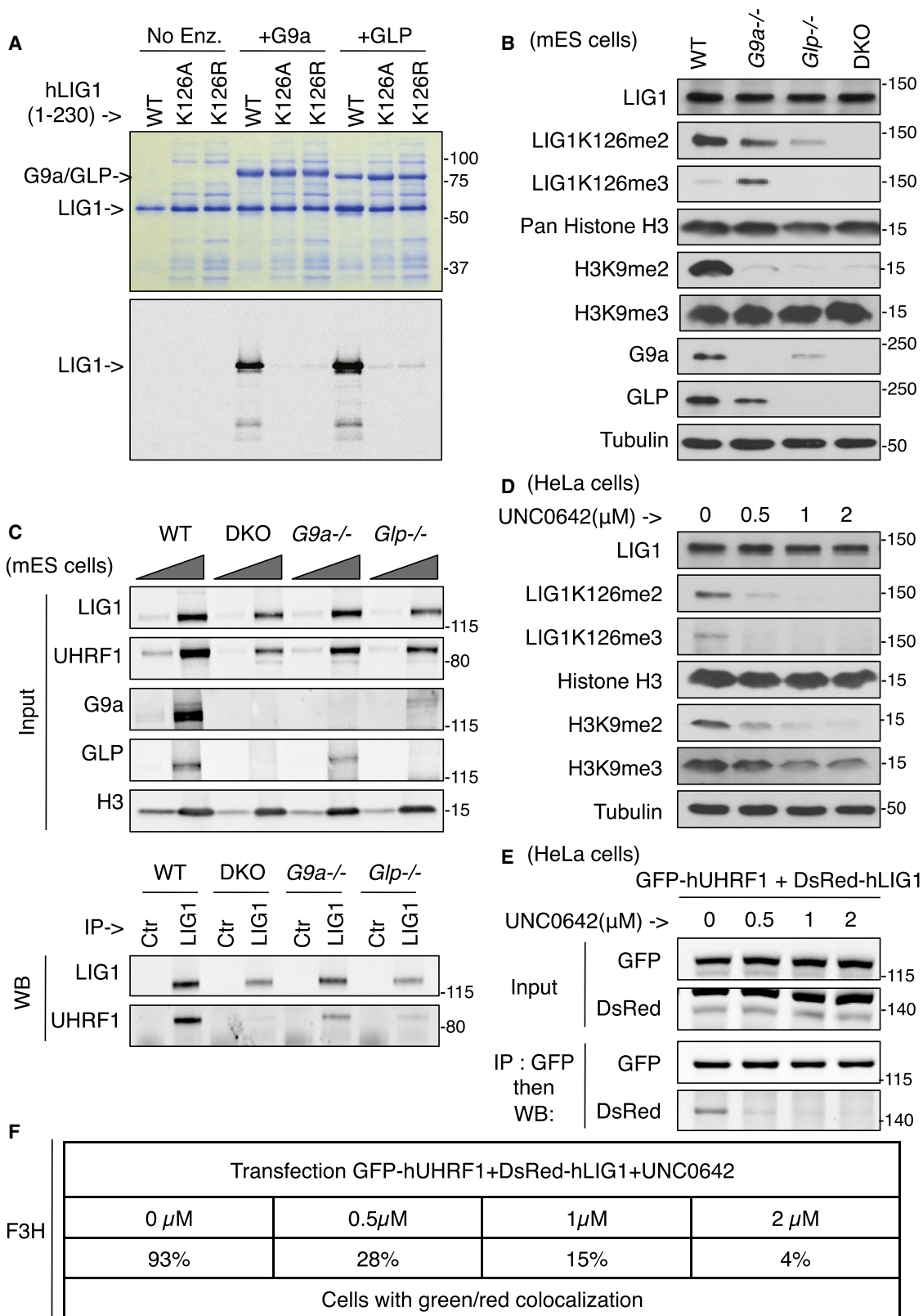
We used the more severely affected cells, with the *Lig1Δ32* allele, for rescue experiments: the methylation defect seen in this cell line was partially rescued by reintroducing WT mLIG1, but much less so by re-expressing a K142R mutant of mLIG1 (Figures S7D, S7E, and S10C).

Finally, we investigated the role of *G9a* and *GLP* in this process. It is known that deletion of *G9a* or *GLP* decreases DNA methylation (Dong et al., 2008; Tachibana et al., 2008); this could be due to an effect on H3K9 methylation, LIG1 methylation, or both. Interestingly, H3K9 methylation is decreased to a similar extent in *Glp*<sup>-/-</sup> and *G9a/Glp* DKO cells (Figure 5B). Therefore, if *G9a* and *GLP* control DNA methylation only by acting on H3K9, then DNA methylation levels should be similar in *Glp*<sup>-/-</sup> and *G9a/Glp* DKO cells. We tested this possibility and observed, instead, that DNA methylation was markedly more reduced in *G9a/Glp* DKO cells compared to *Glp*<sup>-/-</sup> cells (Figure S7F). The loss of DNA methylation—partial in *Glp*<sup>-/-</sup> cells and greater in *G9a/Glp* DKO cells—paralleled the degree of LIG1K126 methylation determined by antibodies and MS (Figures 5B and S5E), supporting the hypothesis that *G9a* and *GLP* regulate DNA methylation at least in part by acting on LIG1.

(D) Model structure, with TTD as light-purple surface model and hLIG1K126me3 peptide as magenta stick model. H3K9me3 peptide, colored in yellow, in TTD:H3K9me3 complex (PDB: 2L3R) is superimposed on the model structure. The model structure is calculated by Modeler (Webb and Sali, 2016) based on the TTD:H3K9me3 complex (PDB: 2L3R).

(E) Magnified view of the binding interface.

See also Figure S4.



(legend on next page)

Together these data show that the UHRF1/LIG1 interaction, promoted by G9a and GLP, is required for efficient DNA methylation maintenance.

## DISCUSSION

### Mechanistic Consequences of UHRF1 Recruitment via LIG1

Our data establish that UHRF1 is recruited to replication sites by LIG1, which contains a histone-like motif, methylated by G9a and GLP, that interacts with the TTD.

This mechanism may have been evolutionarily selected for several reasons. First, in view of the *in vitro* affinities, unassisted recognition of hemi-methylated DNA seems unlikely to suffice for the direction of UHRF1 to hemi-methylated DNA. Of note, our observation that the isolated SRA domain of UHRF1 does not co-localize with replication foci (where hemi-methylated DNA is expected to be found) supports this view. Therefore, recruitment via the replication protein LIG1 may be a more direct and efficient way to target UHRF1 toward recently formed hemi-methylated DNA. The second reason could be to coordinate DNA remethylation and nucleosome formation. It has been shown in the yeast *S. cerevisiae* that DNA ligation on the lagging strand is intrinsically coupled with nucleosome formation (Smith and Whitehouse, 2012). If this phenomenon is conserved in vertebrates, recruitment of UHRF1 by LIG1 might synchronize UHRF1 recruitment to chromatin assembly. The third reason is that UHRF1 could possibly have an important enzymatic function to play at the replication fork, maybe via its ubiquitin ligase activity. For instance, UHRF1 can ubiquitinate histones (Citterio et al., 2004; Nishiyama et al., 2013; Qin et al., 2015), and the interaction with LIG1 may also regulate the timing of this activity. Fourth, the UHRF1/LIG1 interaction might also serve to locally capture and recycle the UHRF1 molecules released by H3K9me2/3-bearing nucleosomes disrupted by the replication fork (Figure 7G). Finally, interaction with LIG1 is a global mechanism that could permit the recruitment of UHRF1 to chromatin irrespective of the existing chromatin marks: for instance, at regions that are depleted of H3K9me2/3.

An immediate question arising from these findings is how UHRF1 might promote methylation maintenance on the leading strand when LIG1, which ligates Okazaki fragments, is enriched on the lagging strand. A first possibility is that UHRF1 might passively diffuse to one or the other strand (model in Figure 7G); indeed, the two replicating strands are held together in close proximity by cohesins. Second, it is possible that the model we describe contributes mostly to methylation maintenance on the lagging strand, and that a different mechanism applies on the leading strand.

### The TTD of UHRF1 Binds a Non-histone Substrate; Properties of the Histone Mimic within LIG1

UHRF1 binds methylated LIG1 peptides with greater affinity than it binds methylated H3 peptides. Structural determination will be required to elucidate the basis for this high-affinity binding, but we speculate that LIG1R121 is involved, as its guanidinium group is in a position to form a hydrogen bond and a salt bridge with UHRF1D142, forming a potentially stronger interaction than H3K4 does (Figure 4E).

We find the affinity of full-length UHRF1 for LIG1K126me2 to be 4-fold higher than its affinity for H3K9me3. However, it is estimated that there are ~60,000 molecules of LIG1 per HeLa cell (Nagaraj et al., 2011), which is at least 50 times less than the number of H3K9me2/3 tails. Therefore the difference in affinity is not sufficient to explain that LIG1 is such a prevalent interactor of UHRF1 in mouse and human cells (Figure 1). The HP1 proteins bind H3K9me2/3 with affinities comparable to UHRF1 (Rothbart et al., 2012), and together they are ~15-fold more abundant than UHRF1 (Nagaraj et al., 2011; Beck et al., 2011). This may explain, in part, the fact that UHRF1 is free to bind LIG1 in cells.

The interaction with LIG1 could be involved in the intramolecular activation of UHRF1. Indeed, two different basic peptides within UHRF1 can bind the TTD and inhibit histone binding: the linker separating the TTD and PHD (Arita et al., 2012; Rothbart et al., 2013), and the poly-basic region (PBR) (Gelato et al., 2014; Zhang et al., 2015; Fang et al., 2016). It is possible that these mechanisms affect LIG1 binding as well; conversely, LIG1 binding could potentially displace these peptides and open up the functional domains of UHRF1. Along these lines, it is noteworthy that binding of hemi-methylated DNA by the SRA can release the TTD and make H3K9me3 binding easier (Fang et al., 2016; Harrison et al., 2016). In our experiments, the presence of hemi-methylated DNA does not increase binding of full-length UHRF1 to LIG1, suggesting that the protein is already in an open conformation. From a functional perspective, it already has been noted that UHRF1 mutants with alterations in the TTD are defective for maintaining DNA methylation in ESCs (for instance, Zhang et al., 2011; Liu et al., 2013b). The phenotypes caused by TTD inactivation were interpreted as being a consequence of impaired H3K9me2/3 binding, but our results show they may also be due to impaired binding to LIG1, or potentially another non-histone interactor. We also note that a recent paper (Zhao et al., 2016) shows a minimal loss of DNA methylation in the liver of mice that have knockin mutations inactivating the TTD. This could suggest that ESCs and adult tissues have different requirements for the function of the TTD.

### Figure 5. The Histone Mimic within LIG1 Is Methylated by G9a and GLP

(A) G9a and GLP methylate hLIG1 *in vitro*; this depends on the presence of K126. Top: Coomassie blue staining of the gel. Bottom: autoradiograph showing the methylation of WT hLIG1, but not the mutant forms, by G9a and by GLP.

(B) G9a and GLP are required for the methylation of LIG1 in mESCs (western blotting).

(C) Deletion of G9a and GLP prevents the LIG1/UHRF1 interaction in mESCs (immunoprecipitation and western blotting).

(D) Treatment of HeLa cells with the G9a/GLP inhibitor UNC0642 abolishes LIG1K126me2 and LIG1K126me3.

(E) Treatment with a G9a/GLP inhibitor prevents the interaction of UHRF1 and LIG1.

(F) Confirmation by the F3H assay.

See also Figures S5 and S9.

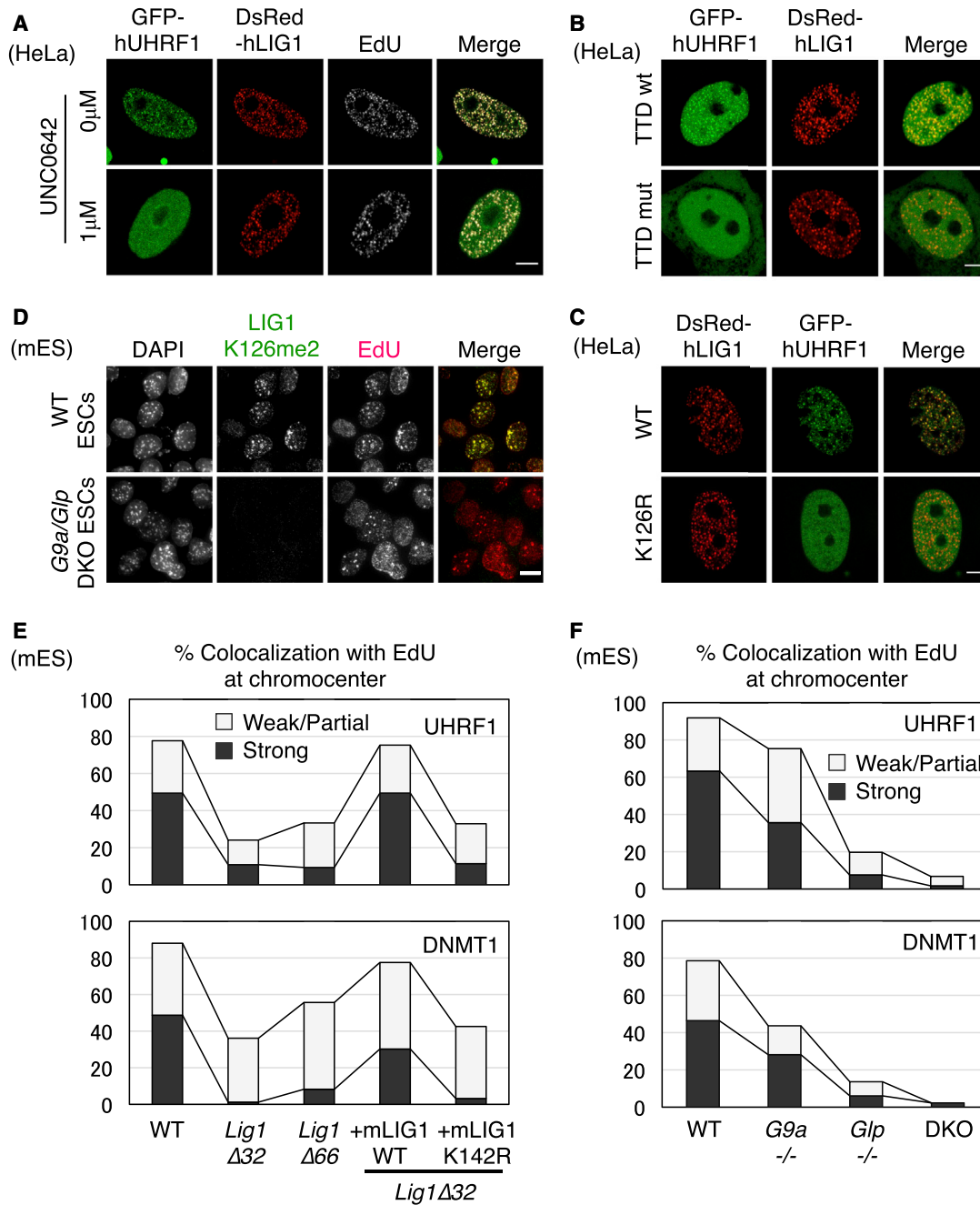


**Figure 6. LIG1K126 and Its Methylation by G9a and by GLP Promote Recruitment of UHRF1 to Replication Foci**

(A) DsRed-hLIG1 and GFP-hUHRF1 co-localize to sites of replication, marked by EdU incorporation. Treatment with a G9a/GLP inhibitor does not affect LIG1 recruitment into replication foci, but prevents UHRF1 recruitment. Cells are HeLa.

(B) The TTD of UHRF1 is sufficient for recruitment to replication sites, and the Y188A/Y191A mutation of the hydrophobic pocket (TTDmut) prevents recruitment. (C) The LIG1K126R mutant is efficiently incorporated into replication foci, but does not promote the recruitment of UHRF1.

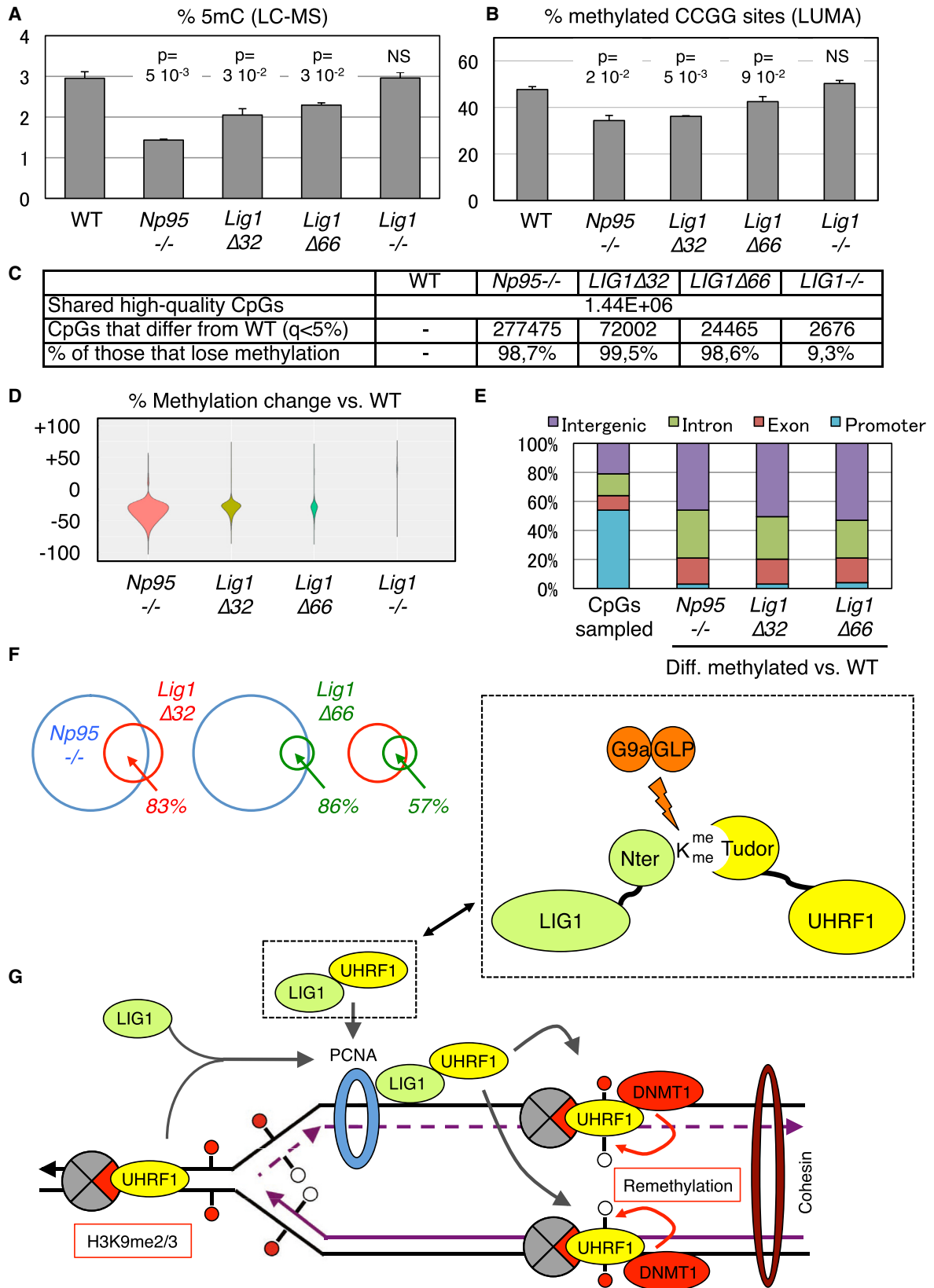
(D) LIG1K126me2 co-localizes with replication sites in mESCs. The signals are not detectable in *G9a/Glp* DKO mESCs. Scale bar, 10  $\mu$ m.

(E) UHRF1 and DNMT1 recruitment to replicating DNA is decreased in cells lacking the LIG1 histone mimic. The re-expression of mLIG1 WT, but not K142R mutant, restores UHRF1 and DNMT1 recruitment. The percentage of cells showing EdU/UHRF1 (upper panel) or EdU/DNMT1 (lower panel) co-localization at chromocenter in the indicated backgrounds is shown.  $n > 300$  cells scored in at least two independent experiments.

(F) UHRF1 and DNMT1 recruitment to replicating DNA is lost following the removal of G9a and GLP, like in (E).

Scale bar, 3  $\mu$ m (A–C).

See also Figures S6 and S10.



(legend on next page)

### Existence of a Potential Backup DNA Methylation Mechanism in *Lig1*<sup>-/-</sup> Cells

We find that UHRF1 is no longer recruited to replicating chromocenters when LIG1 lacks the TARK motif, or when LIG1 is absent altogether; this establishes the key role of LIG1 in UHRF1 localization. We also observe a loss of DNA methylation in ESCs expressing LIG1 variants that cannot interact with UHRF1, consistent with abnormal UHRF1 recruitment in these cells. An unexpected observation, however, is that there is no loss of DNA methylation in cells where LIG1 is completely missing (*Lig1*<sup>-/-</sup> allele). This suggests that these cells have efficient DNA methylation maintenance, even though neither UHRF1 nor DNMT1 are detectably recruited to replicating heterochromatin. We note that dissociation between DNMT1 localization and activity is not unprecedented: a mutant form of DNMT1 that cannot associate with PCNA loses co-localization with replication foci during most of S phase, yet it successfully rescues *dnmt1*<sup>-/-</sup> ESCs (Schermelleh et al., 2007).

What could be the nature of the backup mechanism? We have ruled out some obvious possibilities, such as overexpression of DNMT1 or UHRF1 in *Lig1*<sup>-/-</sup> cells. But we note that LIG3 is coopted for replication when LIG1 function is absent (Le Chalony et al., 2012), which occurs in the *Lig1*<sup>-/-</sup>, but not in the *Lig1* $\Delta$ 32 or *Lig1* $\Delta$ 66 cells. LIG3 does not contain a TARK motif like LIG1, but it does contain BRCT repeats. As the BRCT repeats of BRCA1 are capable of interacting with UHRF1 (Zhang et al., 2016), it might be that LIG3 can recruit UHRF1 with an efficiency too low to be detected by immunofluorescence, but high enough to ensure DNA methylation maintenance.

### G9a and GLP Are LIG1K126 Methyltransferases

G9a and GLP generate H3K9me1 and H3K9me2 in cells; these enzymes also have non-histone targets (Sampath et al., 2007; Rathert et al., 2008; Moore et al., 2013), but in most cases, the functional consequences of non-histone lysine methylation have been difficult to identify. Here we show that the histone mimic within LIG1 is methylated by G9a and GLP, in vitro and in cells. Our experiments using mutant ESCs suggest that GLP is more active than G9a for LIG1 methylation. This order of activity is the opposite of that seen for all other G9a/GLP substrates seen so far, including H3K9, and a future structural determination may help determine the reason for this phenomenon.

We also show that G9a and GLP are necessary for UHRF1/LIG1 interaction and recruitment of UHRF1 to replication foci. Although our data are consistent with LIG1 methylation contributing to UHRF1 and DNMT1 recruitment, we cannot exclude that other functions of G9a/GLP play a role. For instance,

G9a-mediated DNA methylation of retroelements is independent of its H3K9 methyltransferase activity (Dong et al., 2008), and a non-catalytic function may be at play here as well. In addition, our model does not explain why LIG1K126 methylation is increased in *G9a*<sup>-/-</sup> cells, but UHRF1 and DNMT1 recruitment is decreased. Future experiments may help resolve this discrepancy. Notwithstanding these possible caveats, it has been previously observed that the absence of G9a and/or GLP decreases DNA methylation at certain loci in mESCs (Feldman et al., 2006; Dong et al., 2008; Tachibana et al., 2008) and embryos (Auclair et al., 2016). Very recently it has also been shown that the low DNA methylation level of ESCs grown in 2i medium is caused by decreased DNA methylation maintenance, and is accompanied by low G9a/GLP activity (von Meyenn et al., 2016). In all of these cases, the absence of or inactivity of G9a and GLP could cause DNA demethylation because of decreased histone H3K9 methylation, but our results suggest that a contribution of decreased LIG1 methylation could also be involved.

Altogether, our work identifies a new mechanism linking genome and epigenome replication that may be important in normal development but possibly also disease, prompts a reinterpretation of previous models and results, and broadens our understanding of histone mimics and of lysine methyltransferases targeting chromatin proteins.

### STAR★METHODS

Detailed methods are provided in the online version of this paper and include the following:

- KEY RESOURCES TABLE
- CONTACT FOR REAGENT AND RESOURCE SHARING
- EXPERIMENTAL MODEL AND SUBJECT DETAILS
- METHOD DETAILS
  - Generation of stable cell line TAP-Tag purification
  - Mass Spectrometry
  - Purification of recombinant proteins
  - In vitro methylation assay
  - Western blot analysis
  - EdU-labeling combined with Immunostaining
  - Plasmids
  - EMSA
  - Fluorescence polarization assay
  - Isothermal titration calorimetric (ITC) measurements
  - Monoclonal antibodies against methylated forms of LIG1

### Figure 7. The LIG1/UHRF1 Interaction Is Required for Efficient DNA Methylation Maintenance

(A) Decreased 5mC in *Lig1* $\Delta$ 32 and *Lig1* $\Delta$ 66 mutant mESCs (by LC-MS/MS). p value is relative to the WT cells, t test is based on average, and SD is from two independent experiments.

(B) Decreased CCGG methylation in *Lig1* $\Delta$ 32 and *Lig1* $\Delta$ 66 mutant ESCs (by LUMA). Statistics are the same as those used in (A).

(C) RRBS analysis shows loss of CpG methylation in *Lig1* $\Delta$ 32 and *Lig1* $\Delta$ 66 cells.

(D) Violin plot showing the direction and extent of DNA methylation changes relative to WT, for all CpGs with q value <5%.

(E) The distribution of CpGs losing DNA methylation is similar in *Np95*<sup>-/-</sup>, *Lig1* $\Delta$ 32, and *Lig1* $\Delta$ 66 mutant cells.

(F) Venn diagrams illustrate that CpGs that lose methylation after *Lig1* alteration also lose methylation after the deletion of *Np95*.

(G) Summary of our findings. G9a and GLP methylate the LIG1 histone mimic, promoting LIG1/UHRF1 interaction. This stimulates UHRF1 recruitment to replication foci and DNA methylation maintenance.

See also Figure S7.

- ES cell culture
- DNA methylation analysis
- QUANTIFICATION AND STATISTICAL ANALYSIS
- DATA AND SOFTWARE AVAILABILITY

## SUPPLEMENTAL INFORMATION

Supplemental Information includes ten figures and can be found with this article online at <http://dx.doi.org/10.1016/j.molcel.2017.07.012>.

## AUTHOR CONTRIBUTIONS

L. Ferry, A.F., T.T., G.A., T. Shimazu, S.M., O.K., R.A., N.D., T. Suzuki, W.D., M.d.D., L. Fritsch, and S.K. performed the experiments. A.J., H.L., P.H., G.J.F., J.A.M., K.A., Y.S., and P.-A.D. supervised the research. Y.S., T.T., and P.-A.D. wrote the paper.

## ACKNOWLEDGMENTS

For helpful discussions we thank Allison Bardin, Stéphane Marcand, Vincent Pennaneach, Sophie Polo, and Slimane Ait-si-ali. For useful reagents, we thank Denis Biard, Kefei Yu, Sriharsa Pradhan, Christian Bronner, Cristina Cardoso, Thomas Jenuwein, Hitoshi Niwa, Alan Tomkinson, and David Specter. For experiments early in the project, we thank Claudia Darnell Lovell and Solenn Le Guellec. We thank Naohito Nozaki, who developed monoclonal antibodies for methylated LIG1. We thank Masaki Okano for technical advice, useful information, and helpful discussions, and we thank the three reviewers for their suggestions. A.F. was supported by postdoctoral fellowships from Institut National du Cancer (INCa) and Fondation Tourne. T.T. was supported by the RIKEN Junior Research Associate Program. P.-A.D. was supported by the Association pour la Recherche contre le Cancer (ARC2014), Institut National du Cancer (INCa PLBio2010), Groupement des Entreprises Françaises dans la Lutte contre le Cancer (GEFLUC), and Agence Nationale de la Recherche (ANR-15-CE12-0012-01 and ANR-11-LABX-0071/ANR-11-IDEX-0005-01). J.A.M. acknowledges generous support from the Dana-Farber Strategic Research Initiative and NIH (CA042368-30). P.H. was supported by the Medical Research Council (MRC) and the European Research Council (ERC-CoG “dynamicmodifications”), Y.S. acknowledges the RIKEN internal research fund, and H.L. acknowledges support by the Deutsche Forschungsgemeinschaft (DFG; SFB1064/A17).

Received: February 1, 2017

Revised: April 24, 2017

Accepted: July 10, 2017

Published: August 10, 2017

## REFERENCES

- Adelmant, G., Calkins, A.S., Garg, B.K., Card, J.D., Askenazi, M., Miron, A., Sobhian, B., Zhang, Y., Nakatani, Y., Silver, P.A., et al. (2012). DNA ends alter the molecular composition and localization of Ku multicomponent complexes. *Mol. Cell. Proteomics* **11**, 411–421.
- Amouroux, R., Nashun, B., Shirane, K., Nakagawa, S., Hill, P.W.S., D'Souza, Z., Nakayama, M., Matsuda, M., Turp, A., Ndjetehe, E., et al. (2016). De novo DNA methylation drives 5hmC accumulation in mouse zygotes. *Nat. Cell Biol.* **18**, 225–233.
- Arita, K., Isogai, S., Oda, T., Unoki, M., Sugita, K., Sekiyama, N., Kuwata, K., Hamamoto, R., Tochio, H., Sato, M., et al. (2012). Recognition of modification status on a histone H3 tail by linked histone reader modules of the epigenetic regulator UHRF1. *Proc. Natl. Acad. Sci. USA* **109**, 12950–12955.
- Askenazi, M., Parikh, J.R., and Marto, J.A. (2009). mzAPI: a new strategy for efficiently sharing mass spectrometry data. *Nat. Methods* **6**, 240–241.
- Auclair, G., Borgel, J., Sanz, L.A., Vallet, J., Guibert, S., Dumas, M., Cavelier, P., Girardot, M., Forné, T., Feil, R., and Weber, M. (2016). EHMT2 directs DNA methylation for efficient gene silencing in mouse embryos. *Genome Res.* **26**, 192–202.
- Bashtrykov, P., Jankevicius, G., Jurkowska, R.Z., Ragozin, S., and Jeltsch, A. (2014). The UHRF1 protein stimulates the activity and specificity of the maintenance DNA methyltransferase DNMT1 by an allosteric mechanism. *J. Biol. Chem.* **289**, 4106–4115.
- Beck, M., Schmidt, A., Malmstroem, J., Claassen, M., Ori, A., Szymborska, A., Herzog, F., Rinner, O., Ellenberg, J., and Aebersold, R. (2011). The quantitative proteome of a human cell line. *Mol. Syst. Biol.* **7**, 549.
- Berkyurek, A.C., Suetake, I., Arita, K., Takeshita, K., Nakagawa, A., Shirakawa, M., and Tajima, S. (2014). The DNA methyltransferase Dnmt1 directly interacts with the SET and RING finger-associated (SRA) domain of the multifunctional protein Uhrf1 to facilitate accession of the catalytic center to hemi-methylated DNA. *J. Biol. Chem.* **289**, 379–386.
- Bostick, M., Kim, J.K., Estève, P.-O., Clark, A., Pradhan, S., and Jacobsen, S.E. (2007). UHRF1 plays a role in maintaining DNA methylation in mammalian cells. *Science* **317**, 1760–1764.
- Carninci, P., Kasukawa, T., Katayama, S., Gough, J., Frith, M.C., Maeda, N., Oyama, R., Ravasi, T., Lenhard, B., Wells, C., et al.; FANTOM Consortium; RIKEN Genome Exploration Research Group and Genome Science Group (Genome Network Project Core Group) (2005). The transcriptional landscape of the mammalian genome. *Science* **309**, 1559–1563.
- Citterio, E., Papait, R., Nicassio, F., Vecchi, M., Gomiero, P., Mantovani, R., Di Fiore, P.P., and Bonapace, I.M. (2004). Np95 is a histone-binding protein endowed with ubiquitin ligase activity. *Mol. Cell. Biol.* **24**, 2526–2535.
- Cuomo, A., Moretti, S., Minucci, S., and Bonaldi, T. (2011). SILAC-based proteomic analysis to dissect the “histone modification signature” of human breast cancer cells. *Amino Acids* **41**, 387–399.
- Dong, K.B., Maksakova, I.A., Mohn, F., Leung, D., Appanah, R., Lee, S., Yang, H.W., Lam, L.L., Mager, D.L., Schübeler, D., et al. (2008). DNA methylation in ES cells requires the lysine methyltransferase G9a but not its catalytic activity. *EMBO J.* **27**, 2691–2701.
- Du, Z., Song, J., Wang, Y., Zhao, Y., Guda, K., Yang, S., Kao, H.-Y., Xu, Y., Willis, J., Markowitz, S.D., et al. (2010). DNMT1 stability is regulated by proteins coordinating deubiquitination and acetylation-driven ubiquitination. *Sci. Signal.* **3**, ra80.
- Fang, J., Cheng, J., Wang, J., Zhang, Q., Liu, M., Gong, R., Wang, P., Zhang, X., Feng, Y., Lan, W., et al. (2016). Hemi-methylated DNA opens a closed conformation of UHRF1 to facilitate its histone recognition. *Nat. Commun.* **7**, 11197.
- Feldman, N., Gerson, A., Fang, J., Li, E., Zhang, Y., Shinkai, Y., Cedar, H., and Bergman, Y. (2006). G9a-mediated irreversible epigenetic inactivation of Oct-3/4 during early embryogenesis. *Nat. Cell Biol.* **8**, 188–194.
- Felle, M., Joppien, S., Németh, A., Diemer, S., Thalhammer, V., Dobner, T., Kremmer, E., Kappler, R., and Längst, G. (2011). The USP7/Dnmt1 complex stimulates the DNA methylation activity of Dnmt1 and regulates the stability of UHRF1. *Nucleic Acids Res.* **39**, 8355–8365.
- Ficarro, S.B., Zhang, Y., Lu, Y., Moghimi, A.R., Askenazi, M., Hyatt, E., Smith, E.D., Boyer, L., Schlaeger, T.M., Luckey, C.J., and Marto, J.A. (2009). Improved electrospray ionization efficiency compensates for diminished chromatographic resolution and enables proteomics analysis of tyrosine signaling in embryonic stem cells. *Anal. Chem.* **81**, 3440–3447.
- Fritsch, L., Robin, P., Mathieu, J.R.R., Souidi, M., Hinaux, H., Rougeulle, C., Harel-Bellan, A., Ameyar-Zazoua, M., and Ait-Si-Ali, S. (2010). A subset of the histone H3 lysine 9 methyltransferases Suv39h1, G9a, GLP, and SETDB1 participate in a multimeric complex. *Mol. Cell* **37**, 46–56.
- Gelato, K.A., Tauber, M., Ong, M.S., Winter, S., Hiragami-Hamada, K., Sindlinger, J., Lemak, A., Bultsma, Y., Houliston, S., Schwarzer, D., et al. (2014). Accessibility of different histone H3-binding domains of UHRF1 is allosterically regulated by phosphatidylinositol 5-phosphate. *Mol. Cell* **54**, 905–919.
- Gu, H., Smith, Z.D., Bock, C., Boyle, P., Gnirke, A., and Meissner, A. (2011). Preparation of reduced representation bisulfite sequencing libraries for genome-scale DNA methylation profiling. *Nat. Protoc.* **6**, 468–481.

- Harrison, J.S., Cornett, E.M., Goldfarb, D., DaRosa, P.A., Li, Z.M., Yan, F., Dickson, B.M., Guo, A.H., Cantu, D.V., Kaustov, L., et al. (2016). Hemi-methylated DNA regulates DNA methylation inheritance through allosteric activation of H3 ubiquitylation by UHRF1. *eLife* 5, 5.
- Herce, H.D., Deng, W., Helma, J., Leonhardt, H., and Cardoso, M.C. (2013). Visualization and targeted disruption of protein interactions in living cells. *Nat. Commun.* 4, 2660.
- Jeltsch, A., and Jurkowska, R.Z. (2014). New concepts in DNA methylation. *Trends Biochem. Sci.* 39, 310–318.
- Le Chalony, C., Hoffschir, F., Gauthier, L.R., Gross, J., Biard, D.S., Boussin, F.D., and Pennaneach, V. (2012). Partial complementation of a DNA ligase I deficiency by DNA ligase III and its impact on cell survival and telomere stability in mammalian cells. *Cell. Mol. Life Sci.* 69, 2933–2949.
- Levin, D.S., Bai, W., Yao, N., O'Donnell, M., and Tomkinson, A.E. (1997). An interaction between DNA ligase I and proliferating cell nuclear antigen: implications for Okazaki fragment synthesis and joining. *Proc. Natl. Acad. Sci. USA* 94, 12863–12868.
- Lister, R., Pelizzola, M., Dowen, R.H., Hawkins, R.D., Hon, G., Tonti-Filippini, J., Nery, J.R., Lee, L., Ye, Z., Ngo, Q.-M., et al. (2009). Human DNA methylomes at base resolution show widespread epigenomic differences. *Nature* 462, 315–322.
- Liu, F., Barsyte-Lovejoy, D., Li, F., Xiong, Y., Korboukh, V., Huang, X.-P., Allali-Hassani, A., Janzen, W.P., Roth, B.L., Frye, S.V., et al. (2013a). Discovery of an in vivo chemical probe of the lysine methyltransferases G9a and GLP. *J. Med. Chem.* 56, 8931–8942.
- Liu, X., Gao, Q., Li, P., Zhao, Q., Zhang, J., Li, J., Koseki, H., and Wong, J. (2013b). UHRF1 targets DNMT1 for DNA methylation through cooperative binding of hemi-methylated DNA and methylated H3K9. *Nat. Commun.* 4, 1563.
- Moore, K.E., Carlson, S.M., Camp, N.D., Cheung, P., James, R.G., Chua, K.F., Wolf-Yadlin, A., and Gozani, O. (2013). A general molecular affinity strategy for global detection and proteomic analysis of lysine methylation. *Mol. Cell* 50, 444–456.
- Nady, N., Lemak, A., Walker, J.R., Avvakumov, G.V., Karetta, M.S., Achour, M., Xue, S., Duan, S., Allali-Hassani, A., Zuo, X., et al. (2011). Recognition of multivalent histone states associated with heterochromatin by UHRF1 protein. *J. Biol. Chem.* 286, 24300–24311.
- Nagaraj, N., Wisniewski, J.R., Geiger, T., Cox, J., Kircher, M., Kelso, J., Pääbo, S., and Mann, M. (2011). Deep proteome and transcriptome mapping of a human cancer cell line. *Mol. Syst. Biol.* 7, 548.
- Nishiyama, A., Yamaguchi, L., Sharif, J., Johmura, Y., Kawamura, T., Nakanishi, K., Shimamura, S., Arita, K., Kodama, T., Ishikawa, F., et al. (2013). Uhrf1-dependent H3K23 ubiquitylation couples maintenance DNA methylation and replication. *Nature* 502, 249–253.
- Qin, W., Wolf, P., Liu, N., Link, S., Smets, M., La Mastra, F., Forné, I., Pichler, G., Hörl, D., Fellinger, K., et al. (2015). DNA methylation requires a DNMT1 ubiquitin interacting motif (UIM) and histone ubiquitination. *Cell Res.* 25, 911–929.
- Rathert, P., Dhayalan, A., Murakami, M., Zhang, X., Tamas, R., Jurkowska, R., Komatsu, Y., Shinkai, Y., Cheng, X., and Jeltsch, A. (2008). Protein lysine methyltransferase G9a acts on non-histone targets. *Nat. Chem. Biol.* 4, 344–346.
- Rothbart, S.B., Krajewski, K., Nady, N., Tempel, W., Xue, S., Badeaux, A.I., Barsyte-Lovejoy, D., Martinez, J.Y., Bedford, M.T., Fuchs, S.M., et al. (2012). Association of UHRF1 with methylated H3K9 directs the maintenance of DNA methylation. *Nat. Struct. Mol. Biol.* 19, 1155–1160.
- Rothbart, S.B., Dickson, B.M., Ong, M.S., Krajewski, K., Houlston, S., Kireev, D.B., Arrowsmith, C.H., and Strahl, B.D. (2013). Multivalent histone engagement by the linked tandem Tudor and PHD domains of UHRF1 is required for the epigenetic inheritance of DNA methylation. *Genes Dev.* 27, 1288–1298.
- Rottach, A., Frauer, C., Pichler, G., Bonapace, I.M., Spada, F., and Leonhardt, H. (2010). The multi-domain protein Np95 connects DNA methylation and histone modification. *Nucleic Acids Res.* 38, 1796–1804.
- Rozenblatt-Rosen, O., Deo, R.C., Padi, M., Adelmant, G., Calderwood, M.A., Rolland, T., Grace, M., Dricot, A., Askenazi, M., Tavares, M., et al. (2012). Interpreting cancer genomes using systematic host network perturbations by tumour virus proteins. *Nature* 487, 491–495.
- Sampath, S.C., Marazzi, I., Yap, K.L., Sampath, S.C., Krutchinsky, A.N., Mecklenbräuer, I., Viale, A., Rudensky, E., Zhou, M.-M., Chait, B.T., and Tarakhovskiy, A. (2007). Methylation of a histone mimic within the histone methyltransferase G9a regulates protein complex assembly. *Mol. Cell* 27, 596–608.
- Schermelleh, L., Haemmer, A., Spada, F., Rösing, N., Meilinger, D., Rothbauer, U., Cardoso, M.C., and Leonhardt, H. (2007). Dynamics of Dnmt1 interaction with the replication machinery and its role in postreplicative maintenance of DNA methylation. *Nucleic Acids Res.* 35, 4301–4312.
- Schübeler, D. (2015). Function and information content of DNA methylation. *Nature* 517, 321–326.
- Sharif, J., Muto, M., Takebayashi, S., Suetake, I., Iwamatsu, A., Endo, T.A., Shinga, J., Mizutani-Koseki, Y., Toyoda, T., Okamura, K., et al. (2007). The SRA protein Np95 mediates epigenetic inheritance by recruiting Dnmt1 to methylated DNA. *Nature* 450, 908–912.
- Shinkai, Y., and Tachibana, M. (2011). H3K9 methyltransferase G9a and the related molecule GLP. *Genes Dev.* 25, 781–788.
- Silva, J.C., Gorenstein, M.V., Li, G.Z., Vissers, J.P., and Geromanos, S.J. (2006). Absolute quantification of proteins by LCMSE: a virtue of parallel MS acquisition. *Mol. Cell Proteomics* 5, 144–156.
- Smith, D.J., and Whitehouse, I. (2012). Intrinsic coupling of lagging-strand synthesis to chromatin assembly. *Nature* 483, 434–438.
- Tachibana, M., Sugimoto, K., Fukushima, T., and Shinkai, Y. (2001). Set domain-containing protein, G9a, is a novel lysine-preferring mammalian histone methyltransferase with hyperactivity and specific selectivity to lysines 9 and 27 of histone H3. *J. Biol. Chem.* 276, 25309–25317.
- Tachibana, M., Ueda, J., Fukuda, M., Takeda, N., Ohta, T., Iwanari, H., Sakihama, T., Kodama, T., Hamakubo, T., and Shinkai, Y. (2005). Histone methyltransferases G9a and GLP form heteromeric complexes and are both crucial for methylation of euchromatin at H3-K9. *Genes Dev.* 19, 815–826.
- Tachibana, M., Matsumura, Y., Fukuda, M., Kimura, H., and Shinkai, Y. (2008). G9a/GLP complexes independently mediate H3K9 and DNA methylation to silence transcription. *EMBO J.* 27, 2681–2690.
- Unoki, M., Nishidate, T., and Nakamura, Y. (2004). ICBP90, an E2F-1 target, recruits HDAC1 and binds to methyl-CpG through its SRA domain. *Oncogene* 23, 7601–7610.
- von Meyenn, F., Iurlaro, M., Habibi, E., Liu, N.Q., Salehzadeh-Yazdi, A., Santos, F., Petrini, E., Milagre, I., Yu, M., Xie, Z., et al. (2016). Impairment of DNA methylation maintenance is the main cause of global demethylation in naive embryonic stem cells. *Mol. Cell* 62, 848–861.
- Webb, B., and Sali, A. (2016). Comparative protein structure modeling using MODELLER. *Curr. Protoc. Bioinformatics* 54, 5.6.1–5.6.32.
- Zhang, J., Gao, Q., Li, P., Liu, X., Jia, Y., Wu, W., Li, J., Dong, S., Koseki, H., and Wong, J. (2011). S phase-dependent interaction with DNMT1 dictates the role of UHRF1 but not UHRF2 in DNA methylation maintenance. *Cell Res.* 21, 1723–1739.
- Zhang, Z.-M., Rothbart, S.B., Allison, D.F., Cai, Q., Harrison, J.S., Li, L., Wang, Y., Strahl, B.D., Wang, G.G., and Song, J. (2015). An allosteric interaction links USP7 to deubiquitination and chromatin targeting of UHRF1. *Cell Rep.* 12, 1400–1406.
- Zhang, H., Liu, H., Chen, Y., Yang, X., Wang, P., Liu, T., Deng, M., Qin, B., Correia, C., Lee, S., et al. (2016). A cell cycle-dependent BRCA1-UHRF1 cascade regulates DNA double-strand break repair pathway choice. *Nat. Commun.* 7, 10201.
- Zhao, Q., Zhang, J., Chen, R., Wang, L., Li, B., Cheng, H., Duan, X., Zhu, H., Wei, W., Li, J., et al. (2016). Dissecting the precise role of H3K9 methylation in crosstalk with DNA maintenance methylation in mammals. *Nat. Commun.* 7, 12464.

## STAR★METHODS

## KEY RESOURCES TABLE

REAGENT or RESOURCE	SOURCE	IDENTIFIER
<b>Antibodies</b>		
anti-G9a	<a href="#">Tachibana et al. 2005</a>	#8620
anti-GLP	<a href="#">Tachibana et al. 2005</a>	#0422
anti-H3K9me2	<a href="#">Tachibana et al. 2005</a>	#6D11
anti-LIG1	SCBT	N-13
anti-UHRF1	SCBT	sc-98817; RRID: AB_2214278
anti-UHRF1	MBL	Th-10a
anti-DNMT1	SCBT	sc-20701; RRID: AB_2293064
anti-panH3	Millipore	#07-690; RRID: AB_417398
anti- $\alpha$ -tubulin	Sigma	B-5-1-2
anti-LIG1K126me2	MAB Institute	c#60
anti-LIG1K126me3	MAB Institute	d#25
<b>Chemicals, Peptides, and Recombinant Proteins</b>		
IPKRRRTARK (me0, 1, 2 or 3) QLPK 6-FAM (6-Carboxyfluorescein) conjugated to the amino terminus of the peptide	Toray research center	N/A
hUHRF1 TTD (123-285)	<a href="#">Arita et al. 2012</a>	N/A
UNC0642 (G9a and GLP inhibitor)	Sigma	SML1037
H3 peptide (1-30) 6-FAM (6-Carboxyfluorescein) conjugated to the carboxy terminus of the peptide	Toray research center	N/A
<b>Critical Commercial Assays</b>		
Click-iT EdU Alexa Fluor 488 Imaging Kit	Thermo Fisher	C10337
<b>Deposited Data</b>		
Primary western blotting and immunofluorescence data, deposited on Mendeley	This paper	<a href="http://dx.doi.org/10.17632/rky44637gk.1">http://dx.doi.org/10.17632/rky44637gk.1</a>
RRBS data	This paper	GEO: GSE89819
<b>Experimental Models: Cell Lines</b>		
E14 (mouse ES cell line)	N/A	N/A
E14 Np95 <sup>-/-</sup>	<a href="#">Sharif et al., 2007</a>	N/A
E14 LIG1 $\Delta$ 32	This paper	N/A
E14 LIG1 $\Delta$ 66	This paper	N/A
E14 LIG1 <sup>-/-</sup>	This paper	N/A
<b>Recombinant DNA</b>		
pL-CRISPR.EFS.tRFP	Addgene	57819
Mouse LIG1 cDNA	FANTOM collection	AK153993
pL-CRISPR-LIG1 (TGTCTTGAATTGTCCGTTT gRNA)	This paper	N/A
Full-length human UHRF1, HA and Flag-tagged, cloned in retroviral vector pREV	This paper	PAD1466
Full-length human UHRF1, cloned in pEGFPC2	This paper	PAD1543
Full-length human LIG1, cloned in pmRFP-C2	This paper	PAD1766
UbL domain of human UHRF1 (AA 1-83), cloned in pEGFPC2	This paper	PAD 1737
TTD domain of human UHRF1 (AA 116-283), cloned in pEGFPC2	This paper	PAD 1733
PHD domain of human UHRF1 (AA 305-371), cloned in pEGFPC2	This paper	PAD 1734
SRA domain of human UHRF1 (AA 416-591), cloned in pEGFPC2	This paper	PAD 1735
RING domain of human UHRF1 (AA 718-771), cloned in pEGFPC2	This paper	PAD 1736

(Continued on next page)

**Continued**

REAGENT or RESOURCE	SOURCE	IDENTIFIER
Mutated TTD domain of human UHRF1 (Y188A, Y191A??), cloned in pEGFPC2	This paper	PAD 1765
Human UHRF1 with UbL deletion (AA 1-80), cloned in pEGFPC2	This paper	PAD 1742
Human UHRF1 with TTD deletion (AA 133-283), cloned in pEGFPC2	This paper	PAD 1738
Human UHRF1 with PHD deletion (AA 310-366), cloned in pEGFPC2	This paper	PAD 1743
Human UHRF1 with SRA deletion (AA 415-586), cloned in pEGFPC2	This paper	PAD 1744
Human UHRF1 with RING deletion (AA 723-766), cloned in pEGFPC2	This paper	PAD 1745
Nterminal domain of human LIG1 (AA 1-260), cloned in pDsRed	This paper	PAD 1769
Human LIG1 with PBD deletion (AA 1-27), cloned in pDsRed	This paper	PAD 1770
Human LIG1 with TARK deletion (AA 112-178), cloned in pDsRed	This paper	PAD 1785
Software and Algorithms		
trim_galore	<a href="https://github.com/FelixKrueger/TrimGalore">https://github.com/FelixKrueger/TrimGalore</a>	version 0.4.0
bismark	<a href="https://github.com/FelixKrueger/Bismark">https://github.com/FelixKrueger/Bismark</a>	v0.14.3
methylkit R package	<a href="https://github.com/al2na/methylKit">https://github.com/al2na/methylKit</a>	version 0.9.5
R	<a href="https://cran.r-project.org/">https://cran.r-project.org/</a>	v3.2.0

**CONTACT FOR REAGENT AND RESOURCE SHARING**

Further information and requests for resources and reagents should be directed to and will be fulfilled by the Lead Contact, Pierre-Antoine Defossez ([pierre-antoine.defossez@univ-paris-diderot.fr](mailto:pierre-antoine.defossez@univ-paris-diderot.fr)).

**EXPERIMENTAL MODEL AND SUBJECT DETAILS**

We used the following cell lines:

- HeLa. Human cell line, female. Grown in DMEM/10%FBS. Not authenticated for this work.
- HeLaS3. Human cell line, female. Grown in DMEM/10%FBS. Not authenticated for this work.
- HEK293T. Human cell line, female. Grown in DMEM/10%FBS. Not authenticated for this work.
- E14. Mouse ES cell line, male, derived from mouse strain 12910la. Grown in DMEM/15%KSR/LIF. Not authenticated for this work.

**METHOD DETAILS****Generation of stable cell line TAP-Tag purification**

Human UHRF1 was cloned into the retroviral vector, pREV (Fritsch et al., 2010), which contains the HA and Flag tags, and drives expression of the IL2R $\alpha$  receptor on the surface of infected cells. pREV-UHRF1 and its empty counterpart were used to infect HeLa XLP cells; these cells are HeLa S3 derivatives expressing a murine receptor (MCAT-1) that permits infection by murine retroviruses.

Infected HeLa-XLP cells were selected using magnetic beads. Dynabeads CD25 (Invitrogen) bind to IL2R $\alpha$  expressed on the surface of positive cells, and the selection was achieved using a magnet. HeLa-XLP cells were scraped, collected in a Falcon tube and centrifuged 5min at 1400 rpm. 2mL of DMEM 10% FBS, 1% PS + 7.5  $\mu$ L of magnetic beads (for cells in a petri dish of 10cm of diameter) were added in a 5mL tube. After the wash, beads were re-suspended in 0,5mL medium. The pellet of HeLa-XLP was re-suspended in 3mL medium and 0,5mL of beads suspension was added. After 1h of incubation at room temperature positive cells (bound by magnetic beads) were selected using a magnet. Two washes with medium were made to avoid the presence of negative cells. Selected cells were re-suspended in 2mL medium and plated in a well of a 6-well plate. Cells with beads were observed in the microscope. Another selection of positive cells was made after ten days. After selection, the cells were grown in suspension, and 10 g of cells were used for immunopurification.

In the first step, the cells were resuspended in a hypotonic buffer (10 mM Tris-HCl pH 7.65; 1.5 mM MgCl<sub>2</sub>; 10 mM KCl) and disrupted with 20 strokes of a tight-fitting Dounce homogenizer. The cytosolic fraction was separated from nuclei by 7 min centrifugation at 4°C at 9000 rpm. The “Nuclear soluble” fraction was obtained by incubation of the nuclear pellet in a high salt buffer (900 mM NaCl, 20 mM Tris pH 7.65, 25% glycerol, 1.5 mM MgCl<sub>2</sub>, 0.2 mM EDTA), to get 300 mM NaCl, for 30 min at 4°C and centrifugation at 10,000 rpm. The resulting pellet, which corresponds to the “Chromatin” fraction, was resuspended and digested with micrococcal nuclease (Sigma) until it consisted primarily of mononucleosomes. Nuclear soluble and chromatin fractions were then ultracentrifuged at 32000 rpm for 1 hr at 4°C in a Beckman SW-T32 rotor. Tagged complexes were then purified by immunoprecipitation using anti-FLAG antibody immobilized on agarose beads (cat# A2220, Sigma). After elution with the FLAG peptide, the bound complexes containing nucleosomes were further affinity purified on anti-HA antibody-conjugated agarose (cat# A2095, Sigma) and eluted with the HA peptide. An aliquot of the double-immunopurified complexes were resolved on 4%–12% SDS-PAGE bis-Tris acrylamide gradient gels in MOPS buffer (Invitrogen), and stained using the SilverQuest kit (Invitrogen). The rest of the eluted complexes were used for MS analysis.

### Mass Spectrometry

Tandem Affinity Purified UHRF1 samples were reduced with 10 mM DTT for 30 min at 56°C in the presence of 0.1% RapiGest SF (Waters). Cysteines were alkylated with 22.5 mM iodoacetamide for 20 min at room temperature in the dark. Samples were digested overnight at 37°C with 4 μg trypsin (Promega). Tryptic peptides were acidified and purified by batch mode reversed phase and strong cation exchange chromatography (Adelmant et al., 2012). Purified peptides were divided in two aliquots and analyzed in two independent nanoLC-MS runs (Ficarro et al., 2009). Peptides were loaded onto a precolumn (4 cm POROS 10R2, Applied Biosystems) and eluted with an HPLC gradient (NanoAcquity UPLC system, Waters; 2%–35% B in 45 min; A = 0.2 M acetic acid in water, B = 0.2 M acetic acid in acetonitrile). Peptides were resolved on a self-packed analytical column (12 cm Monitor C18, Column Engineering) and introduced in the mass spectrometer (LTQ Orbitrap Velos, Thermo Scientific) equipped with a Digital PicoView electrospray source platform (New Objective, ESI spray voltage = 2.2 kV). The mass spectrometer was programmed to perform data-dependent MS/MS on the ten most abundant precursors in each MS1 scan using alternating collision induced and higher energy dissociation (CID and HCD respectively, with 35% normalized collision energy). Dynamic exclusion was enabled with a repeat count of one and exclusion duration of 30 s. MS spectra were recalibrated using the background ion (Si(CH<sub>3</sub>)<sub>2</sub>O)<sub>6</sub> at m/z 445.12 ± 0.03 and converted into a Mascot generic file format (.mgf) using multiplier scripts (Askenazi et al., 2009). Search parameters included trypsin specificity with up to two missed cleavages, fixed carbamidomethylation (C, +57 Da) and variable oxidation (M, +16 Da). Precursor mass tolerance was set to 10 ppm and product ion mass tolerances were set to 0.5 Da and 0.2 Da for CID and HCD spectra, respectively. The search databases consisted of human protein sequences (downloaded from RefSeq on 07/11/2011) and protein sequences for common lab contaminants both appended to their own decoy database. Sequence matches to the decoy databases were used to implement a global 1% false discovery rate (FDR) filter for the resulting peptide identifications. A fast peptide matching algorithm was used to map peptide sequences to all possible human genes. We discarded candidate proteins that were detected in a large compendium of negative TAP controls with a frequency greater than 1% (Rozenblatt-Rosen et al., 2012). Protein abundances were estimated following the method described by Silva et al. (2006) averaged over the two replicate LC-MS/MS runs and normalized to the abundance of UHRF1 in each TAP sample.

### Purification of recombinant proteins

*Escherichia coli* BL21 (pLysS) strains were transformed with pET-28b plasmids, and the bacteria were cultured in 2x YT medium with antibiotics and 0.5 mM isopropyl β-D-1-thiogalactopyranoside (IPTG) for 16 hr at 16°C. The cells were pelleted and lysed with 1xPBS/0.5% NP-40 by sonication with a Branson Sonifier (S-250D, Branson Ultrasonics) for 10 min on ice. The lysates were centrifuged at 7,300 xg for 10 min, and the supernatants were incubated with Ni-NTA Agarose (QIAGEN) for 1 hr at 4°C with gentle rotation. The agarose beads were washed 5 times with wash buffer (50 mM Tris-HCl, pH 7.5, 20 mM imidazole) and then eluted with elution buffer (50 mM Tris-HCl pH 7.5, 250 mM imidazole). The purified proteins were dialyzed with 1xPBS/10% glycerol, and the concentration was measured using the Bradford Protein Assay Kit (BioRad Laboratories). GST-G9a and GLP SET domain were prepared as described in the literature (Tachibana et al., 2001).

### In vitro methylation assay

One microgram of recombinant His-LIG1 proteins were incubated in reaction buffer (50 mM Tris-HCl pH 8.0) with GST-G9a SET or -GLP SET (1 μg) and 14C-labeled SAM (0.01 μCi, Perkin Elmer) for 2 hr at 30°C. The reaction was stopped by adding Laemmli SDS-sample buffer. Proteins were resolved on acrylamide SDS-PAGE gel, and the dry gel was exposed to an imaging plate (FUJI-FILM) for 24 hr to 48 hr, and the autoradiographic signal was detected using a BAS-5000 Image analyzer (FUJI-FILM).

### Western blot analysis

Cells were harvested after trypsinization, washed twice with PBS, and lysed with lysis buffer (50 mM Tris-HCl at pH 7.5, 150 mM NaCl, 1 mM EDTA, 10% glycerol, 0.5% Triton X-100, 1 mM DTT, 1 mM phenylmethanesulfonyl fluoride, and 1x protease inhibitor cocktail; Nacalai). The cell lysates were subjected to the Bradford Protein Assay Kit (BioRad Laboratories). Equivalent amounts of protein were resolved by SDS-PAGE and then transferred to nitrocellulose membrane.

### EdU-labeling combined with Immunostaining

ES cells ( $4.0 \times 10^4$ ) were seeded on  $\mu$ -Slide Chamber (ib81201, Ibdid) which was pre-coated with 10  $\mu$ g/mL of laminin. After overnight culture, the cells were incubated with 20  $\mu$ M EdU (5-ethynyl-2'-deoxyuridine) for 10 min at 37°C, washed with PBS twice and fixed with 4% paraformaldehyde for 20 min at room temperature (RT). After fixation, the cells were permeabilized with 0.2% Triton X-100 in PBS for 10 min at RT and then incubated with Click reaction solution (4 mM CuSO<sub>4</sub>, 4.8  $\mu$ M Alexa Fluor Azide 555, 10 mM sodium ascorbate, in 1xPBS) for 30 min at RT with protection from light. After Click reaction, the cells were incubated with 3% BSA/0.2% Tween-20 in 4xSSC for 30 min at RT and with primary antibody for 2 hr at 37°C (for UHRF1) or RT (for LIG1 and DNMT1). After washing twice with 4xSSC, the cells were incubated with secondary antibodies conjugated with Alexa Fluor 488 for 1h at 37°C or RT, washed with 4xSSC twice, and finally mounted with ProLong Diamond Antifade Mountant with DAPI (P36961, Thermo Fisher Scientific). Images were obtained using a DeltaVision microscope (Corns Technologies). UHRF1, DNMT1, or LIG1 co-localization with EdU-signal was assessed at DAPI-dense regions.

### Plasmids

Plasmids were generated using PCR and restriction enzymes, or Gibson Assembly Cloning. All plasmids were sequenced prior to use. Mouse LIG1 was amplified from a FANTOM clone (Carninci et al., 2005).

### EMSA

Expression and purification of TTD (123-285) and mutant derivatives (Y188A/Y191A and D142A) was described previously (Arita et al., 2012). LIG1 peptide concentration was 4  $\mu$ M, and a 0.5–3.0-fold molar amount of the TTD was used. Samples were incubated for 30 min at 4°C in binding buffer (20 mM Tris-HCl (pH 7.5), 150 mM NaCl, 1 mM DTT, and 10% (w/v) glycerol). The complexes were then run at 4°C on a 7.5% polyacrylamide gel (Supersep, Wako, with running buffer: 25 mM Tris containing 12.5 mM boric acid (pH 8.8)). The proteins were then detected by staining with Coomassie Brilliant Blue.

### Fluorescence polarization assay

Fluorescence polarization assays for interaction between LIG1 peptide and TTD were performed in binding buffer (20 mM Tris-HCl (pH 7.5), 150 mM NaCl, 10% glycerol, 1 mM DTT, and 0.05% Tween 20) at 25°C using a Synergy2 plate reader (Biotek Japan). The excitation and emission wavelengths were 485 nm and 522 nm, respectively. The 6-Carboxyfluorescein Hydrate (FAM) labeled LIG1 peptide (10 nM) was incubated with increasing concentrations of the TTD. Curve-fitting analyses and dissociation constant ( $K_d$ ) were conducted using ORIGIN software version 8.0 (OriginLab). The observed data were fitted to the equations assuming a 1:1 binding stoichiometry ratio.

### Isothermal titration calorimetric (ITC) measurements

A MicroCal LLC calorimeter, VP-ITC, was used for the ITC measurements. UHRF1 TTD123-385 was dissolved into the ITC buffer (10 mM Tris-HCl (pH 7.5), 150 mM NaCl, 1 mM DTT), and lyophilized LIG1 peptides were dissolved in the same buffer. The TTD solution (5  $\mu$ M) in the calorimetric cell was titrated with the peptide solution (62.5  $\mu$ M) at 298 K. The data were analyzed with the software ORIGIN (MicroCal) using one-site model.

### Monoclonal antibodies against methylated forms of LIG1

LIG1K126me<sub>2</sub>- and me<sub>3</sub>-specific mouse monoclonal antibodies were generated by immunizing with the corresponding peptides (MAB Institute). For detection of LIG1K126me<sub>2</sub>, the c#60 clone was used in the data presented here. Other clones (c#43, #46 and #64) were used for validation of the results from c#60. For detection of LIG1K126me<sub>3</sub>, the d#25 clone was used in the data presented here. An independent clone, d#2, was used for validation of the results obtained with d#25.

### ES cell culture

The WT and *Np95*<sup>-/-</sup> cells are in the E14 background (Sharif et al., 2007). All cells were grown in DMEM with 15% Knockout Serum Replacement (KSR, GIBCO), and LIF. Mutagenesis of *Lig1* in the E14 background was done by CRISPR with the guide RNA TGCTTGAATTGTCGTTT cloned in plasmid pL-CRISPR.EFS.tRFP (Addgene #57819).

### DNA methylation analysis

Southern blotting, LUMA and Pyrosequencing were done according to standard procedures.

RRBS was done and analyzed according to a published protocol (Gu et al., 2011). LC-MS was as in a previous paper (Amouroux et al., 2016).

### QUANTIFICATION AND STATISTICAL ANALYSIS

The details of quantification and statistical methods used can be found in each figure legend.

**DATA AND SOFTWARE AVAILABILITY**

The primary western blotting and imaging data for this paper have been deposited to Mendeley Data and are available at <http://dx.doi.org/10.17632/rky44637gk.1>.

The RRBS data were submitted to the GEO repository under accession number GEO: GSE89819.